Mechanically-Induced Intercellular Remodeling of Cardiomyocytes by Magnetic Micromanipulation
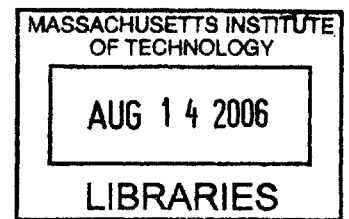
by

J.P. Michael Motion

B.S. Electrical Engineering
Massachusetts Institute of Technology, 2004

Submitted to the Department of Electrical Engineering and Computer Science
in Partial Fulfillment of the Requirements for the Degree of

Master of Engineering in Electrical Engineering and Computer Science
at the
Massachusetts Institute of Technology

February 3, 2006

Signature of Author: _____
Department of Electrical Engineering and Computer Science
February 3, 2006

Certified by: _____

Alan J. Grodzinsky
ıedical Engineering
Professor of Γ'˗˗˗˗·˗˗˗ ˑ ˑ˗ˑ˗˗˗˗˗ ˑ ˑ ˑ ˑ ˑ ˑ ıcal Engineering
ıesis Supervisor

Certified by: _____

Richard T. Lee
A˗˗˗˗ˑ˗˗ Uˑˑˑˑˑˑˑ ˑˑ Medicine Harvard Medical School
ˑupervisor

Accepted by: _____

C. Smith
Cnaırman, Deparunenı Commıttee Graduate Theses

Mechanically-Induced Intercellular Remodeling of Cardiomyocytes by Magnetic Micromanipulation

by

J.P. Michael Motion

Submitted to the Department of Electrical Engineering and Computer Science on February 3, 2006 in Partial Fulfillment of the Requirement for the Degree of Master of Engineering in Electrical Engineering and Computer Science

Abstract

Gap junctions are responsible for providing and maintaining a pathway for intercellular communication. This is critical in the heart where gap junctions are responsible for maintaining electrical impulse propagation. Connexin43 (Cx43) is the most abundant gap junction in the heart, and studies have shown that spatial heterogeneity of Cx43 may promote electrical instability and anisotropic conduction pathways that may cause cardiac arrhythmias. Structural and electrical remodeling of gap junctions have been linked to increases in stresses in conditions such as hypertrophy. Understanding how local mechanical forces influence the remodeling of gap junctions can provide insight into arrhythmias and reentry circuits. In this work, I describe a system for exerting local mechanical forces on cardiomyocytes to study gap junction remodeling and I show that cell-to-cell movement and subsequent remodeling of Cx43 can occur. The system consisted of patterned linear strands on polyacrylamide gels and mechanical stimulation using magnetic micromanipulation. Cardiomyocytes were patterned on polyacrylamide gel using 25µm and 50µm microchannels. Mechanical stimulation was induced in sections with high densities of magnetic beads. With a maximal input current of 1.5A, the system generated 1.5nN at 100µm distance from the magnetic trap, and this was sufficient to induce cell-to-cell movement. Cell-to-cell movement was measured to be $0.032\pm0.03\mu m/min$, three times faster than the average cell-to-cell movement under no applied force. Remodeling of Cx43 was also shown using Cx43-YFP transfected cells while a local force induced cell–to-cell movement. Changes in both the distribution and expression of the protein were seen throughout time as the linear strand was pulled by the magnetic force. We conclude that this system can induce remodeling of Cx43 by an applied local force. This work establishes a system to allow to quantification of applied mechanical loads and resultant Cx43 remodeling.

Thesis Supervisor: Alan J. Grodzinsky
Title: Director, Center for Biomedical Engineering
      Professor of Electrical, Mechanical, and Biological Engineer

Thesis Supervisor: Richard T. Lee
Title: Associate Professor of Medicine, Harvard Medical School

Acknowledgement

First and foremost, I would like to thank my thesis advisors, Dr. Richard Lee and Prof. Alan Grodzinsky, for their guidance, support and commitment. I am grateful to have found a great lab that has taught me so much about biology, cardiology and research. The past three years have been a great journey filled with exciting ideas and projects which included heart regeneration, gap junction remodeling and cardiac electrophysiology. I am deeply grateful to Dr. Richard Lee for allowing me to be part of his lab, for teaching me the systematic approach to science and for his constant motivation and encouragement to pursue research and feel excited and passionate about science.

I would also like to thank all the members of Dr. Richard Lee's Laboratory for their support, motivation and encouragement and for making my time at the lab a very enjoyable and fun experience. I am very grateful to Hayden Huang and Jan Lammerding for their guidance, support, advice and long conversations about science and engineering, and for their commitment to helping me plan and review my experiments. I am also grateful to Mike Davis and Patrick Hsieh who were the first to introduce me to cardiovascular research and teach me about cell culture and surgical procedures. I would also like to acknowledge the help of Thomas Gervais, who kindly provided me with microfabrication techniques and materials for the linear strand patterning.

I owe my gratitude to my girlfriend, parents, and relatives for their constant love, support and encouragement. That is why I would like to dedicate my thesis to my mother Josiane, my grandparents, Raymond and Germaine, my girlfriend Emyluz, my aunt and uncles, Elizabeth, Rolando, Raymond and Gilbert, and my cousins Rolando and Ricardo whom throughout my 5 years at MIT have guided, counseled, and supported me every single step of the way.

Table of Contents

Chapter 1

1.1 Introduction

An important area in cardiovascular research is understanding how structural and electrical remodeling lead to anisotropic conduction pathways that degenerate into heart failure. Experimental and clinical evidence suggest that changes to the spatial distribution of the major ventricular gap junction protein, connexin43 (Cx43), can lead to altered patterns of conduction, arrhythmias and electrical instability of the heart [1, 2]. Studies have further examined the role of gap junctional remodeling in physiological conditions such as hypertrophy and heart failure. In both heart failure and decompensated hypertrophy, Cx43 is downregulated and redistributed within cardiomyocytes [1]. Nonetheless, in compensated hypertrophy, Cx43 is upregulated [1]. Differences in stresses and forces might lead to such dynamic variations of gap junction remodeling. However, the sequence of events that leads to this active remodeling is not fully understood. There is a need to develop quantitative models that will yield insight on how mechanical forces regulate the spatial heterogeneous expression of connexin 43 in order to gain new insights on reentry circuits and arrhythmias in remodeling myocardium.

Different techniques have been used to study the effects of applied forces on cellular dynamics such as optical tweezers, unipolar magnets and stress chambers. However, none of them are suitable to study the dynamics and requirements for cardiac remodeling. A more sophisticated system and technique must be design that will allow for the spatial and temporal control and orientation of an applied force. The focus of this thesis is thus

to develop a system capable of inducing cell-to-cell movement and remodeling of gap junctions in cardiomyocytes. Toward this end, I make the following contributions. First, a magnetic micromanipulation system was setup to apply localized forces on magnetic beads and mechanically induced cell-to-cell movement. The system consisted of a temperature controlled stage that maintained the temperature to approximately $37^{\circ}C$, a perfusion system to control the pH to 7.4 and a magnetic trap that exerted a localized force on cardiomyocytes. A soft polyacrylamide gel substrate was patterned on glass coverslips and used to reduce cell-to-substrate force interactions. Microchannel patterning techniques were developed to pattern on polyacrylamide gel for positioning and aligning cardiomyocytes parallel to each other. Finally, an auto shutter system and a high-speed piezo z-drive system for nanofocusing and scanning were used to acquire three dimensional time lapse stacks of the remodeling system. Algorithms were developed for analyzing the images of the stack. Experiments with this system showed that cell-to-cell movement is possible, as well as remodeling of the gap junctions on a section with high concentration of magnetic beads. These and other results will be further discussed in Chapter 7.

1.2 Thesis Organization

The following chapters will provide a more detailed description of the methods and approaches used for developing and testing the cardiac remodeling system. Chapter 2 provides an overview of the necessary background to understand the biology of gap junctions and cardiac remodeling. Chapter 3 explains the theory and design of the

magnetic trap system, while Chapters 4 and 5 explain the patterning protocols for the polyacrylamide gel and the cardiac linear strands. Chapter 6 provides the methods for the force remodeling experiments and Chapter 7 discusses and analyzes the cell-to-cell movement and remodeling results. Finally, Chapter 8 proposes future experiments and improvements with the proposed remodeling setup.

Chapter 2

2.1 Biological Overview

More than a century ago, the idea of local remodeling was introduced. The concept proposed that a cell's fate was to die alone even though cells live together in organized multilayers of tissue [3]. Thus, cell death was not considered a collective event. This notion of local remodeling has intrigued scientists and researchers. Detachment of cells, either by death or other external factors, produces a cascade of signaling events that can lead to cellular death [3].

Understanding the relationship between cellular changes and tissue remodeling has been a challenge. Molecular biologists have extensively mapped and characterized intercellular signaling pathways. However, how these signaling pathways are integrated into the actual 3D remodeling of tissues remains unexplained. This is extremely important in heart disease, where remodeling of the myocardium is an important determinant of potentially lethal arrhythmias. Thus, there is a need to develop a model to quantify localized remodeling effects on cell-to-cell communication and coupling.

This thesis proposes a new method to study local remodeling of gap junctions in heart cells, as a means to understand how remodeling myocardium can establish the milieu for disturbed conduction through the cardiac tissue. Before describing this model, we will provide an overview of the biology needed to understand the model and the clinical relevance of the project.

2.2 Cardiac Cells

Cardiac myocytes, or cardiomyocytes, are among the largest cells in the body, usually 20μm wide and 100μm in length, and can grow up to 120μm in length [4]. In culture, with minimal tensile load, they usually have a width of about 10-15μm and a length of 50μm. Cardiomyocytes are composed of bundles of myofibrils, which are thin, elongated structures. Each myofibril consists of thin filaments and thick filaments; thin filaments are composed of actin, and the thick filaments are composed of myosin. Repeating microstructures, known as sarcomeres, are periodically positioned and joined via Z-lines within the myofibrils to provide mechanical contraction. The shortening and expansion of the sarcomeres causes myocytes to contract during cardiac excitation and contraction coupling. This is the process by which an action potential triggers the cell to contract through the influx and outflux of calcium ions [4].

Within the heart, cardiomyocytes are positioned next to each other via sarcolemma connections through the intercalated disk. The intercalated disk contains 3 specialized junctions: gap junctions, desmosomes and adherens junctions. These junctions are responsible for maintaining proper cell communication. Gap junctions facilitate proper impulse propagation to maintain electrical stability in the heart, while the desmosomes and adherens junctions ensure mechanical transmission of the traction generated by the individual myocytes throughout the myocardium.

2.3 Intercellular Communication and Gap Junctions

Intercellular communication is vital for growth, function and synchronization of cellular processes [3, 5]. It is through the maintenance and regulation of intercellular communication that organs function properly. Intercellular communication can occur in different ways. It is mediated either by soluble extracellular ligands in endocrine, paracrine or autocrine interactions, or by intercellular junctions.

In mammalian cells, intercellular junctions are known as gap junctions. They control a number of biological functions such as the passage and flow of metabolites, ions and molecules smaller than 1kD from cell-to-cell. They are responsible for providing and maintaining a pathway for cell-to-cell electrical and metabolic communication. This is particularly important in excitable tissues, such as the heart, where gap junctions are responsible for the electrical stability of their conduction system. Any alteration to the distribution and quantity of the gap junctions can have an adverse effect on conduction, either by increasing or decreasing local conduction velocities and, in some cases, producing reentry pathways that allow rapid tachyarrhythmias [6, 7]. Furthermore, gap junctions are crucial in controlling vasomotor tone for embryonic development and patterning; transporting molecules to cells distant from blood vessels; and in the immuno-inflamatory pathology [3, 8].

Gap junctional channels are formed by two hexameric connexons. A connexon is formed by six connexin subunits, arranged hexagonally as a hemi-channel, that docks to another connexon at specific regions of the plasma membrane of adjacent cells [3, 5]. Once a

gap junction forms, it tends to stay open for seconds to minutes, and is closed by high concentrations of calcium and by low pH [9].

Gap junctions are tissue and cell-type specific. The distribution and type of gap junction varies and depends on the types of connexin forming the junction. The gap junction might consist of identical connexins, known as a homomeric channel, or of two or more different connexins subunits, known as a heteromeric channel [10]. Since there are approximately 20 genes for connexins in both humans and mice, there are many possible gap junction combinations [3, 5, 10].

An interesting aspect of connexins is their remarkably short half-life. One would expect that this important element for stabilizing the heart's electrical system would have a long half-time and turnover rate. However, experimental evidence suggests that connexins are highly dynamic and have a very high turnover rate and short half-life. In cultured cells, most connexins have a half-life of only 1 to 4 hours, and it is expected that the same is true *in vivo* [11]. This high turnover rate leads to the hypothesis that a short half-life provides a means for regulatory intervention to compensate for changes in synthesis or degradation rates [11].

2.4 Gap Junctions in the Heart

Gap junctions are vital for the electrical stability and conduction of the heart. They are responsible for the propagation of the cardiac action potential and synchronization of

contraction by regulating the flow of ionic currents through them [12-14]. The number and type of gap junctions are both factors that determine the speed propagation [15]. The type of gap junction varies depending on the location in the heart. In general, cardiac gap junctions are located at the intercalated disk. In a normal heart, most gap junctions are localized parallel to the long axis of the cell, although in some cases they can be found perpendicularly to the long axis of the cell, allowing for both longitudinal and transverse conduction [16]. Since increased number of gap junctions leads to higher ionic currents and conduction velocity, the longitudinal conduction is much faster than the transverse [17].

Primarily, four different connexin genes are expressed in the heart. These are connexin37 (Cx37), connexin40 (Cx40), connexin43 (Cx43) and connexin45 (Cx45) [3, 5, 16]. Cx37 is expressed in endothelial cells of the endocardium, aorta and coronary vessels [18, 19], whereas Cx40 is co-expressed with Cx43 in the atria and in the ventricular conduction system where Cx43 colocalizes with Cx45; and Cx45 is expressed in the AV, ventricles and in some locations within the atria [16, 20]. Cx43 is the most abundant isoform in mammalian hearts, expressed in all myocytes of the atria and ventricles and usually located in the intercalated disk (see Figure 1). Cx43 plays a critical role in stabilizing the electrical conduction system in the ventricles [16]. Numerous studies have suggested that the reduction or closure of Cx43 gap junctions causes slower conduction and may lead to arrhythmias [12, 13, 21]. Furthermore, irregular distribution of Cx43 can also lead to arrhythmias and reentry pathways [22].
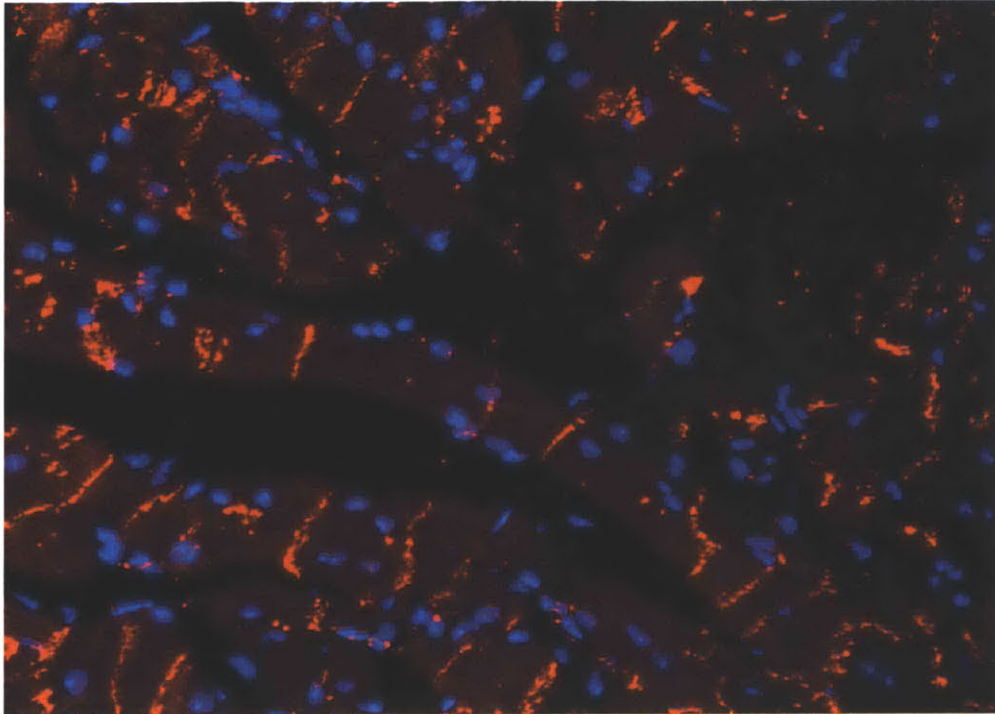
Figure 1: Gap junctions in the heart. Cx43 is mostly localized along the end of the longitudinal axis of cardiomyocytes at the intercalated disk. Cx43, shown in red, was stained using a monoclonal anti-connexin43 antibody (Sigma) at a 1:100 dilution followed by a 1:200 dilution of Alexa Fluor conjugated IgM (Molecular Probes), and nuclei, shown in blue, was stained with a 1:1000 dilution of DAPI.

2.5 Gap Junctions in Neonatal Cardiac Myocytes

Since mammalian adult cardiac cells do not survive *in vitro* for long periods of time (generally hours), most experimental studies on Cx43 are performed using cultured neonatal rat ventricular myocytes, which can survive for days to weeks. Neonatal rat cardiac myocytes retain their electrical activity for long periods of time [16]. Neonatal cardiac myocytes spontaneously beat, in contrast to adult cardiac cells that have less spontaneous activity.

The distribution of gap junctions in neonatal cardiac myocytes differs from that of adult myocytes. Neonatal cardiac myocytes express Cx40 and Cx43, but express Cx45 in small amounts [16, 23]. The quantity of Cx40 has a temporal dependence and decreases with culture time. The reason for this decrease is not well understood. As a result, neonatal cardiac myocytes are probably not an ideal model to study changes in Cx40. In contrast, the pattern of Cx43 expression is less variant. By using anti-Cx43 antibodies, Kwak et al. showed identical patterns of dot-like labeling at appositional cell borders at different culture densities and time points [23]. However, in contrast to adult myocytes, in which Cx43 gap junctions are at the intercalated disk, Cx43 are expressed at cell-cell contacts of neonatal cells. The expression pattern appears to be around the perimeter of the cells, and is not located in specific regions as in adult cardiac cells as shown in Figure 2. However, in the remodeled tissue surrounding an infarcted section in the heart, the distribution of gap junctions is similar to the neonatal dot-like expression [24].
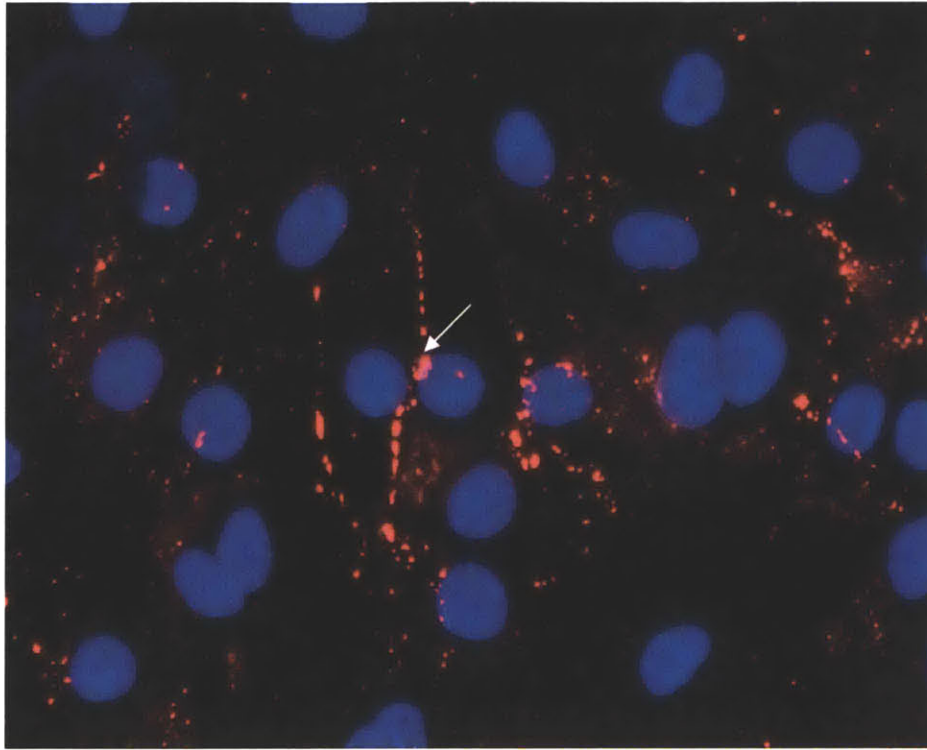
Figure 2: Distribution of Cx43 in isolated neonatal ventricular rat cardiomyocytes at 40X. A dot-like expression is seen around the border of the cells. Cx43 is shown in red, and nuclei are shown in blue and were stained as described in Figure 1.

2.6 Intercellular Communication and Impulse Propagation

Intercellular communication plays a key role in maintaining the electrical stability of the heart. Gap junctions facilitate rapid and coordinated electrical excitation to maintain normal rhythmic contraction. Furthermore, they are responsible for maintaining the communication contacts between neighboring cells. Besides gap junctions, several other factors play a key role on impulse propagation. For instance, impulse propagation is influenced by the electrical properties of the myocytes that generate the action potential [25]. Action potential generation is driven by three major current ionic flows: calcium (Ca^{2+}), sodium (Na^-) and potassium (K^+). The influx and outflux of these currents change

the membrane capacitance and potential, and elicit the action potential. This relationship is described by the following mathematical equation [26]:

$$\frac{dV}{dt} = -\frac{1}{C} I_{ion} \ .$$

It states that the change in the membrane potential is equal to the negative of all transmembrane ionic currents carried by the ionic channels and other membrane mechanisms divided by the value of the membrane capacitance. Thus, any alteration to any ionic channel will change the electrical behavior of the cell's action potential generation. Finally, the heart's two and three dimensional anisotropic morphology and structure influences the direction and shape of the electrical propagation waveform [25, 27, 28]. Any alterations to this structure, such as hypertrophic enlargement or infarction, will destabilize the impulse propagation. Several models have been developed to describe impulse propagation. In the following section I will briefly discuss them in an effort to highlight the importance of gap junctional coupling in propagation of the electrical depolarization wave through the myocardium.

2.6.1 Single Cell Chain Model

The single cell chain impulse propagation model consists of a chain of myocytes electrically stimulated to model impulse propagation. The model assumes that the cells are only coupled at adjacent cells and that the propagation is purely longitudinal by eliminating any anisotropic conduction that might have resulted from lateral localization

of gap junctions. Due to discontinuities in the conduction and impulse propagation within the strand, the model only describes the time of impulse propagation between two neighboring cells. In experiments carried out by Fast et al. on synthetic neonatal strands, impulse propagation was measured between two neighboring cells using high-resolution optical mapping to detect changes in the intensity of voltage sensitive dyes and reconstruct transmembrane potential. From these experiments, the average delay for the impulse to propagate across the border is around 80μsecs and around 38μsecs to propagate 30μm inside the cytoplasm [29], clearly indicating that the propagation across cell borders is proportional to the propagation within the cell.

2.6.2 Anisotropic Cellular Network Model

The heart consists of elongated coupled cardiac myocytes in a three dimensional substrate, but the pattern is comprised of spiraling sheets of myocytes. Within this substrate, multiple cell types other than cardiomyocytes, such as endothelial cells and fibroblasts from microvessels and connective tissue, couple to cardiomyocytes [25]. The multiple cell lines have different electrical properties that alter the conduction velocity and waveform of the propagation. Conduction velocity and impulse propagation is much faster in the ventricle than in the atria, mainly because of the amount and type of gap junctions present in both regions. Thus, there are many factors that cause electrical coupling to be anisotropic and heterogeneous.
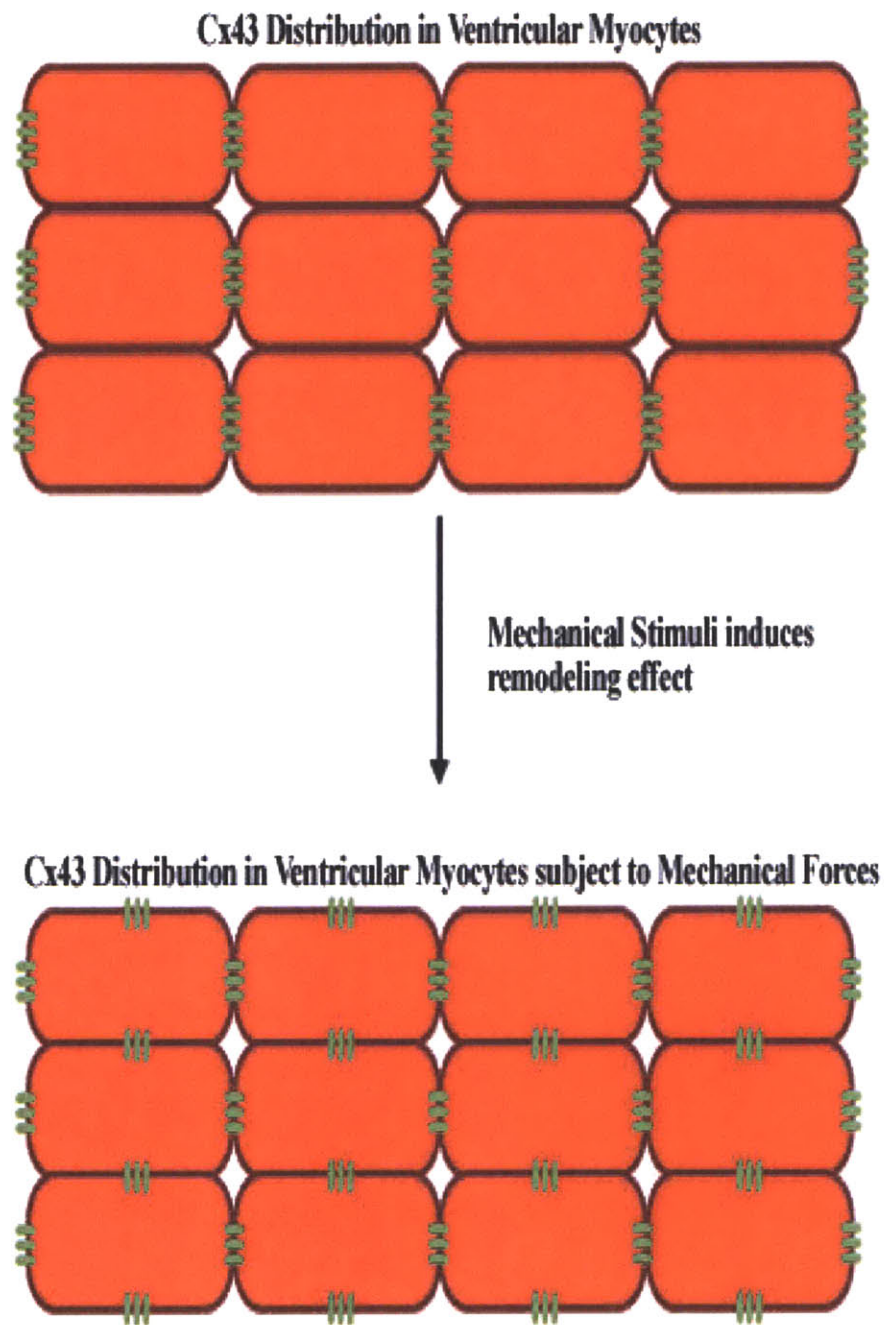
With these considerations and building upon the single cell chain model, the anisotropic cellular network model combines the different parameters and elements, such as cell type and size, and gap junction and ion channels distribution, for modeling anisotropy [25]. The additional elements aid the illustration of the relationships between the impulse propagation characteristics and the region of the heart in which the impulse is propagating. Such a model can be modified to account for the differences in gap junction density across the atria, ventricles, and SA node. Furthermore, by modeling the multiple chains of cells in parallel, the effects of discontinuities in propagation imposed by longitudinal gap junctions are eliminated by the introduction of lateral gap junctions. Spach et al. simulated the intracellular excitation sequence in an anisotropic cellular network model and found that the propagation velocity within a cell is not constant, but spatially variant on the distribution of gap junctions. The local conduction velocity decreases vertically as the profile approaches cell borders, where ionic currents can exit the cell through gap junctions. At the same time, the profile increases longitudinally as the propagation approaches the cell's end and the longitudinal intercalated disk [30]. As a result, the propagation profile resembles a parabolic flow.

This model provides insight into how different conduction direction promotes anisotropy, since anisotropy is dependent on conduction and impulse propagation direction. Thus, we can obtain a ratio for anisotropic conduction by taking the ratio of longitudinal conduction velocity in cells relative to their transversal velocity [25]. This anisotropy ratio provides information about the electrical stability of the heart and can be used to

identify reentry pathways [31]. In general, the higher the anisotropy ratio, the more electrically stable the heart is.

Different factors can alter anisotropy in cardiac myocytes. Since the generation of an action potential is dependent on the total ionic currents flowing through the membrane, changes in the ionic channels will alter action potential generation and impulse propagation; hence, the anisotropy. At the same time, changes in cell size and morphology will alter conduction speeds. For instance, an increase in the longitudinal axis of a cell will increase the activation delay, reduce longitudinal conduction velocities, and decrease the anisotropy ratio, promoting an increase in discontinuous conduction pathways. A reduction of cell size would have the opposite effect [17].

Finally, changes in gap junction amount and distribution will also lead to changes in anisotropy [25]. As previously described, most gap junctions are located longitudinal to the cells axis at the intercalated disk. Since there is a correlation between gap junction location and impulse propagation, any changes in the position of the gap junctions will influence the propagation waveform. For instance, if a cell's gap junctions remodel as shown in Figure 3, reducing the amount of junctions at the longitudinal direction and increasing the amount of junctions in the transverse direction, the anisotropy will likely decrease because the longitudinal conduction will reduce and the transverse conduction will increase.

20

Cx43 Distribution in Ventricular Myocytes

Mechanical Stimuli induces remodeling effect

Cx43 Distribution in Ventricular Myocytes subject to Mechanical Forces

Figure 3: Changes in gap junction distribution will change the anisotropy of the section and induce remodeling. When subject to pulsatile stretch, for instance, Cx43 expression is upregulated in both the longitudinal and transverse expression as shown by Zhuang et al. [32]. In this example, the anisotropy would decrease since conduction velocities will propagate in both the longitudinal and transverse directions.

2.7 Effects of Connexin Remodeling on Impulse Propagation and Cardiac Function

Connexins have an important role for ensuring proper electrical propagation in myocardium. Impulse propagation and conduction velocity in cells is regulated by intercellular conductance, cytoplasm resistance and gap junction resistance. Gap junction resistance depends on the type of connexin forming the junction. As a result, any alteration or modification to the connexins in the junction and to the number and distribution of the junctions will affect the conduction velocity and impulse propagation.

High resolution optical mapping has demonstrated that heterogeneous Cx43 expression is closely associated with electrophysiological heterogeneities across the transmural ventricular wall and can contribute to arrhythmic substrates [33]. Furthermore, in Cx43 +/- mice, a 50% reduction in Cx43 corresponded to a 25% reduction in conduction velocity [34, 35]. Heterozygous deletion of Cx43 also leads to a modest decrease in conduction velocity and increases the probability of arrhythmias after ischemia [36]. When chimeric mice were made with Cx43 deficient embryonic stem cells, mice developed normally, however conduction pathways were abnormal in the epicardium and the contractility was depressed [13]. Thus, heterogeneous Cx43 expression has profound implications for myocardial function.

2.8 Distribution of Gap Junctions in Cardiac Diseases

Changes in distribution and expression levels of gap junctions occur in most myocardial diseases [2, 16]. For instance, in hypertensive rats, the expression of Cx40 is

significantly increased and the levels of Cx43 are decreased [16, 37]. In hypertrophied human left ventricles and ischemic hearts, the levels of Cx43 are decreased by 40%, with no changes in gap junction size [38]. Also, in a guinea pig model of congestive heart failure, Cx43 was decreased by 37% at the congestive heart failure stage [39].

One of the most common alterations is remodeling of the gap junctions from the longitudinal intercalated disk to the lateral cell borders [40], changing local anisotropy and altering conduction pathways. This redistribution has been seen in hibernating myocardium, hypertrophy, and ischemia [41-44]. In some cases, this shift of gap junctions from longitudinal to lateral borders is associated with reentry. For instance, redistribution of Cx43 at the border zone of infarcts correlates with the presence of reentrant circuits [45].

An important factor in remodeling of gap junctions in cardiac diseases is phosphorylation of connexins, which acts as an important modulator of cardiac conduction. Normally, Cx43 exists in a phosphorylated state. However, during cardiac diseases such as ischemia the uncoupling of the gap junctions is associated with dephosphorylation of Cx43 and accumulation of unphosphorylated Cx43 in the gap junctions [46]. Furthermore, hereditary cardiomyopathic hamsters express an increase in phosphorylation of Cx43 on tyrosine residues that correlate to a reduction in conduction [47].

It is clear that most arrhythmias and cardiac diseases are associated with some remodeling of the gap junctions. Gap junctional changes include increase and reduction of connexin levels as well as increased lateralization of the gap junctions. It is unclear, however, how remodeling contributes to the changes in conduction since in some cardiac conditions, such as in decompensated hypertrophy and infarcts, the lateralization of the connexins does not contribute to the cell-to-cell communication network and should not play a pivotal role in the impulse propagation [41, 48]. Nonetheless, gap junctional remodeling does alter conduction velocities and are present in arrhythmias and hypertrophy.

2.9 Mechanotransduction and Cardiac Hypertrophy

Mechanotransduction is a signaling response to cellular mechanical stimulation. Cardiac myocytes are subject to constant mechanical stresses to which they respond depending on the intensity of the stimulation. Mechanosensors allow cardiomyocytes to respond to increased levels of stress and strain through several pathways that mediate mechanotransduction. Rapid mechanical changes are controlled by calcium release, while longer mechanical stresses stimulate long term structural changes including cellular hypertrophy through many signaling pathways.

Cardiac hypertrophy is a long term response to increased loading condition in an attempt to restore systolic functions [49]. It is characterized by an enlargement in the heart usually due to an increase in the size of the differentiated cardiomyocytes. Initially, the

hypertrophic response compensates for the additional mechanical stress. The enlargement of the tissue normalizes the increase in wall pressure and restores cardiac function. However, if the mechanical stimulus is increased or prolonged, it will lead to decompensated hypertrophy and cardiac failure [50]. Different mechanisms are responsible for the development of cardiac hypertrophy such as stretch-induced growth factors. Cardiac hypertrophy often is accompanied by increased expression of embryonic genes, disturbed calcium dynamics of cardiomyocytes and increased interstitial collagen synthesis that leads to fibrosis [51]. Furthermore, there is a clear difference in connexin expression in hypertrophy. Compensated hypertrophy, in patients with aortic stenosis, is characterized by an increase in Cx43 lateral localization and an upregulation in overall Cx43 expression, whereas decompensated hypertrophy is characterized by a reduction in Cx43 [1]. Although there is no clear explanation for the different distribution of Cx43, it is plausible that the upregulation in Cx43 might represent an adaptive response to the increase mechanical stress, whereas the downregulation in decompesated hypertrophy might be early signs of heart failure.

2.10 Effects of Structural and Electrical Remodeling in Hypertrophy

2.10.1 Structural Remodeling in Hypertrophy

Mechanical forces from pathological stresses such as hypertension and volume and pressure overload often lead to structural remodeling in the heart. Cells and tissue adjust to these stresses by changing cell size and gap junction positions until a new pathological steady-state is achieved.

During the process of hypertrophy, as cells increase in size, local positional remodeling might occur as cells shift relative to each other to counter the increase in stress. This regulated feedback mechanism in response to stress might influence the distribution of local gap and adherens junctions, such as N-cadherin, which is necessary for the formation of Cx43 gap junctions [52]. As a result, local displacement and repositioning of cells might correlate with the transient breakdown and reorganization of the gap junctions.

Several studies have demonstrated the effect of stress on cardiac cells. For instance, Zhuang et al. showed that Cx43 and N-cadherin are upregulated in cardiomyocytes in response to pulsatile stretch [32]. In patients with aortic stenosis, Cx43 was upregulated and relocalized to the lateral borders, whereas in patients with decompensated hypertrophy, there was a marked reduction in Cx43 [1]. Furthermore, *in vitro* experiments have shown that stretch activates numerous signaling pathways inducing the release of angiotensin II, endothelin-1, vascular endothelial growth factor and transforming growth factor [53-55], all of which cause an increase in the expression of Cx43 in cardiomyocytes [56]. This suggests that gap junctions and other adherens junctions must be able to remodel dynamically in response to local stresses. This concept is supported by the finding that the half-life of Cx43 is very short, which would allow gap junctions to remodel quickly in response to stimuli.

2.10.2 Electrical Remodeling in Hypertrophy

Electrical remodeling refers to electrophysiological disturbances that alter the electrical and impulse propagation of the heart during structural remodeling. Several factors are responsible for the electrical remodeling in hypertrophy. For instance, changes in genes encoding sarcolemmal ion channels and electrogenic transporter alter AP elicitation, propagation and recovery time during hypertrophy [57].

Electrical remodeling in hypertrophy may be driven by changes in transmembrane Ca^{2+} fluxes, which may lead to action potential prolongation [57]. Armoundas et al. proposed that the magnitude of the L-type Ca^{2+} current is inversely related to the degree of hypertrophy since the magnitude is increased in mild-to-moderate hypertrophy, but remains constant in severe hypertrophy [58]. As a result, there is a correlation between the cellular and molecular phenotype and the degree of hypertrophy. For instance, pressure overload hypertrophy is characterized by an increased Ca^{2+} transient and an inward Ca^{2+} current that might generate a positive feedback mechanism to further stimulate the hypertrophy. At the same time, the inactivation of the recovery period of the inward Ca^{2+} current is accelerated and levels of NCX protein and transcripts are downregulated, resulting in a decrease of NCX function, both of which might induce remodeling of the sarcolemmal Ca^{2+} [59]. In volume overload hypertrophy, however, NCX activity is increased, which increases the sarcolemmal Ca^{2+}, and the K^+ current is decreased. These alterations in ionic currents can affect the resting membrane potential, maximum diastolic potential or action potential prolongation and refractoriness, contributing to abnormal automaticity in hypertrophied hearts.

2.11 Clinical Relevance

Cardiac hypertrophy is a process that can sometimes degenerate into heart failure, which has serious complications, including death. It is clear that the regulation of the heart's electrical system depends on the stability and integrity of the ionic pumps and gap junctions responsible for eliciting and propagating the action potential. Thus, understanding the mechanisms of hypertrophy, both structural and electrical, is a milestone that cardiovascular researchers and electrophysiologists are trying to accomplish. To this date, there is no clear indication of what initiates the hypertrophic stimuli and how this initial and local stimulus disturbs the distribution of ions and gap junctions. Cells might respond to this stimulus locally and transiently, or it might be an all or none response. To be able to identify and determine how local forces remodel the structural and electrical characteristics of the cell might provide the insights into electrical remodeling. For example, understanding how these local forces and remodeling occur may allow identification of signaling pathways that might link hypertrophy and arrhythmias.

Chapter 3

3.1 Mechanotransduction Techniques

In order to study the remodeling effects of gap junctions, cells must be stimulated to induce local displacements. Several techniques have been developed to induce mechanical stresses on cells. For instance, micropipette aspiration has been frequently used to study local deformation of single cells [60]. Unipolar magnetic traps and magnetic tweezers have been used to study the properties of cell membranes [61]. Fluid shear chambers, and stretching of elastic substrates have also been used to study global effects of remodeling [32, 62]. However, these techniques are not suitable for studying cell-to-cell remodeling or local remodeling in cardiomyocytes. The system that must be developed needs to model the anisotropic characteristic of the heart and be able to manipulate single cells, or a small group of cells, in order to quantify the effects of local forces, in terms of magnitude and orientation, to the remodeling of the gap junctions.

3.2 Magnetic Micromanipulation System

The goal of the magnetic micromanipulation system is to develop an experimental remodeling system where local forces can be applied to single cells to quantitatively measure cell-to-cell coupling and remodeling effects. The system must also dynamically capture the spatial remodeling throughout time and maintain a proper environment that will not cause additional remodeling effects. This is particularly important since

connexin channels are sensitive to pH, and cardiomyocytes need to be maintained at 37°C.

3.2.1 Design of Magnetic Trap

Controlling a magnetic field is crucial for manipulating cells with magnetic beads. One of the most critical aspects of this design was producing a magnetic field with a high gradient, primarily because superparamagnetic beads react to the gradient of the magnetic field. Superparamagnetic beads only have a dipole moment when exposed to a magnetic field and once the dipole appears, the gradient of the field exerts a force on the beads. Therefore, the most practical approach was to design an electromagnet that could be closely positioned to the regions of interest.

My collaborators, Dr. Huang and Dr. Lammerding [63, 64], designed the magnetic trap to apply high magnetic forces up to 10nN to cells loaded with superparamagnetic beads. When designing the trap, several factors were taken into account. For instance, the tip geometry was designed to gain maximum maneuverability within a 35mm dish. The size and geometry of the core were modified to fit onto a MX100R micromanipulator (SD Instruments, OR) and provide additional z-plane movement. It was also designed to protect against corrosion by plating the trap core and tip with a very thin layer of gold and/or nickel coatings.

In theory, the magnetic trap is a basic magnetic circuit that uses the fundamental principle of Ampere's Law [65]:

$$\oint B \cdot ds = \mu_o i$$

which states that the line integral of the magnetic field around a closed loop is proportional to the electric current flowing through the loop. If it is assumed that the core material of the magnetic trap has an infinite permeability, then the magnetic flux density B in the core is proportional to the magnetic field intensity H as shown by:

$$\lim_{\mu \to \infty} B = \mu H$$

If fringing effects and leakage fluxes are neglected, then the magnetic field will only be nonzero at the tip of the magnetic trap. Using ampere's circuital law, the magnitude of the magnetic field is then proportional to the total current running through the wires by:

$$\oint H \cdot dl = Ht = Ni$$

where t is the end area of the tip, N is the number of turns in the core, and i is the magnitude of the current running through the wire. Thus, the intensity of the magnetic field will be strictly related to the current and number of turns in the core.

Since we want to obtain the highest force possible, we want to maximize the number of turns by selecting the smallest wire possible, considering that the maximum practical number of wire layers is 5. We must also take under consideration the total electrical resistance of the windings which can impact the output current of the power supply if the load imposed by the winding is greater than 80Ω. It was found that any wire, ranging from AWG15-AWG30, was suitable for the design since the smallest wire, AWG30, would have a total electrical resistance of ~74Ω.

The final consideration taken for selecting the wire size was heat dissipation. Heat dissipation is important particularly because the tip of the magnetic trap would be positioned a few microns away from cardiomyocytes, which are temperature sensitive. Although AWG30 would yield the largest ampere-turns, it would also yield the largest thermal dissipation. It was a design objective to minimize the power dissipation on the wires so that the temperature on the tip of the magnetic trap was below 37°C, while maximizing the ampere-turns to obtain approximately 500 ampere-turns. Since thermal resistivity is proportional to the ratio of the length of the wire over the cross sectional area as shown below:

$$R = \frac{\rho L}{A}$$

where ρ is resistivity, L is length, and A is cross sectional area, then a smaller wire will have a high thermal resistivity. However, since we are trying to keep the magnetic trap cool, a high thermal resistivity is not desirable. Therefore, by looking at the thermal

resistivities and looking at the possible ampere-turns for a given wire, AWG18 had the lowest theoretical thermal resistivity and would yield the highest ampere-turns for our design.

The magnetic trap was manufactured at the MIT machine shop. It was made from CMI-C Iron (CMI Specialty Products, CT), which has a high permeability and low coercivity. The trap was annealed to improve the magnetic characteristics and coated with nickel and/or gold to protect against corrosion. The iron core was then wrapped using AWG18, mounted onto the MX1005 micromanipulator, and connected to the HP 65454A power supply, as shown in Figure 4. Since the HP power supply is current limited to 1.5A, the current magnetic trap can be driven at a maximum of 1.5A.

Figure 4: Magnetic trap. The magnetic trap is mounted on a manual micromanipulator at an angle of ~45° to ensure that the tip is parallel to the cells.

3.2.2 Force Equations on Superparamagnetic Beads

Superparamagnetic beads were chosen because of their higher magnetic content and the ease of attaching proteins, such as fibronectin, to them. The force acting on a superparamagnetic bead is proportional to the gradient of the cross product of the magnetic field intensity as shown below:

$$F = \mu_o \chi V \nabla (H \times H)$$

where μ_o is the permeability constant, χ is the volume susceptibility, V is the volume of the magnetic bead and H is the magnetic field intensity. Thus, the force exerted on a bead is dependent primarily on the field's gradient and intensity, and saturates depending on the magnetic properties of the core and magnetic beads. The intensity of the magnetic field is limited by the power supply since the source is current-limited and H is proportional to source's output current. The magnetic trap's tip geometry was optimized to maximize the gradient and was designed having a flat, square tip parallel to the surface of the cells.

3.2.3 Characterization of Magnetic Trap

To characterize the magnetic trap, two calibrations were performed, one for force generation and the other to control for the trap's operating temperature. The force calibration was set up to determine the relationship of the spatial distribution of forces on beads and the input current. The calibration was performed as described by Huang et al.

34

[63]. 4.5μm super-paramagnetic beads (Dynabeads M-450, Invitrogen) were suspended in 70% ethanol, air dried in a 35mm polystyrene dish, and resuspended in dimethylpolysiloxane (DMPS-12M, Sigma), which has a kinematic viscosity of 12,500 centistokes. The magnetic trap was then inserted into the dish and positioned far from the surface and the bottom of the dish. After waiting a few minutes for the system to stabilize, the magnetic trap was turned on and the beads were tracked. The calibration was performed for currents ranging from 0.6A to 1.5A, with 3 measurements as a minimum for each setting. The force on the bead was calculated using Stoke's formula for low Reynolds numbers flow:

$$F = 6\pi\mu VR$$

in which μ is the dynamic viscosity of the fluid, V is the velocity of the bead at steady state and R is the radius of the bead. A MATLAB (Mathworks) program, written by Dr. Lammerding, performs a regression on all data sets for a given current setting to calculate the best square-fit line of the force spatial distribution. The calibration showed that that magnetic force decreases rapidly with distance as shown by Figure 5.
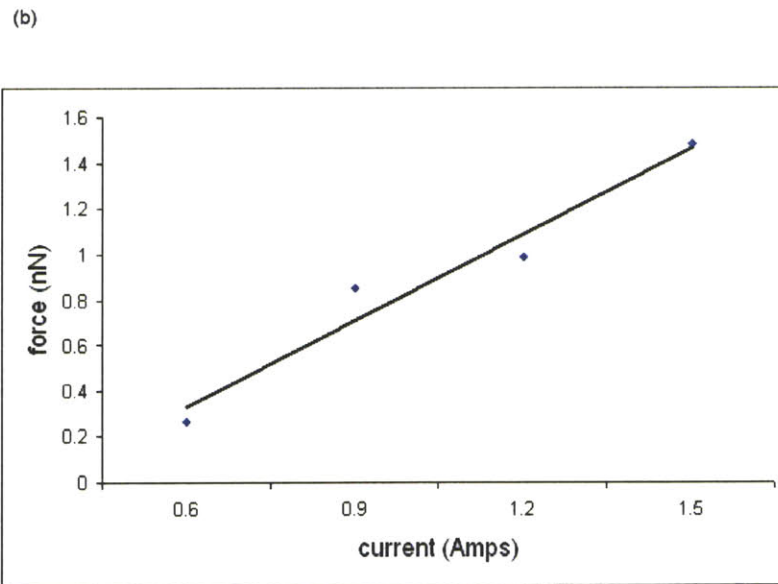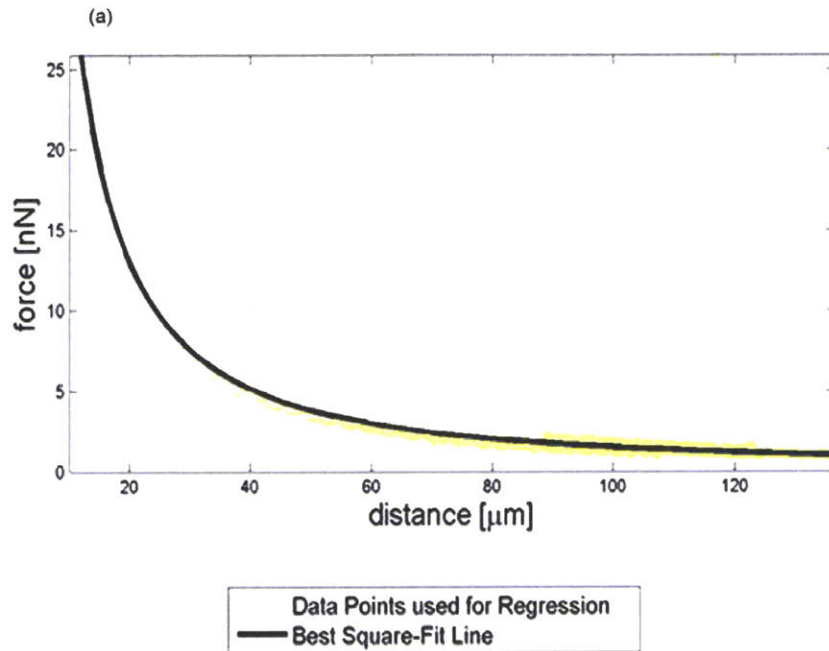
Figure 5: Magnetic trap calibration results. (a) 1.5A yields the strongest force as expected. The spatial distribution of the force decreases rapidly with increasing distance from the magnetic trap. (b) The force exerted on a bead decreases with lower currents. At 100μm, the greatest force, 1.49nN, is generated by an input current of 1.5A. At 0.6 A, the force generated is low, 0.27nN.

To ensure that the temperature of the magnetic trap did not exceeded 37°C, a temperature calibration was performed. Using a digital thermometer (51II, Fluke, WA), the temperature on both the magnetic trap's core and tip were measured while the magnetic trap was running at the maximum current of 1.5A. The calibration showed that after 4 hours, the core and tip temperatures were below 30°C, as shown in Figure 6.
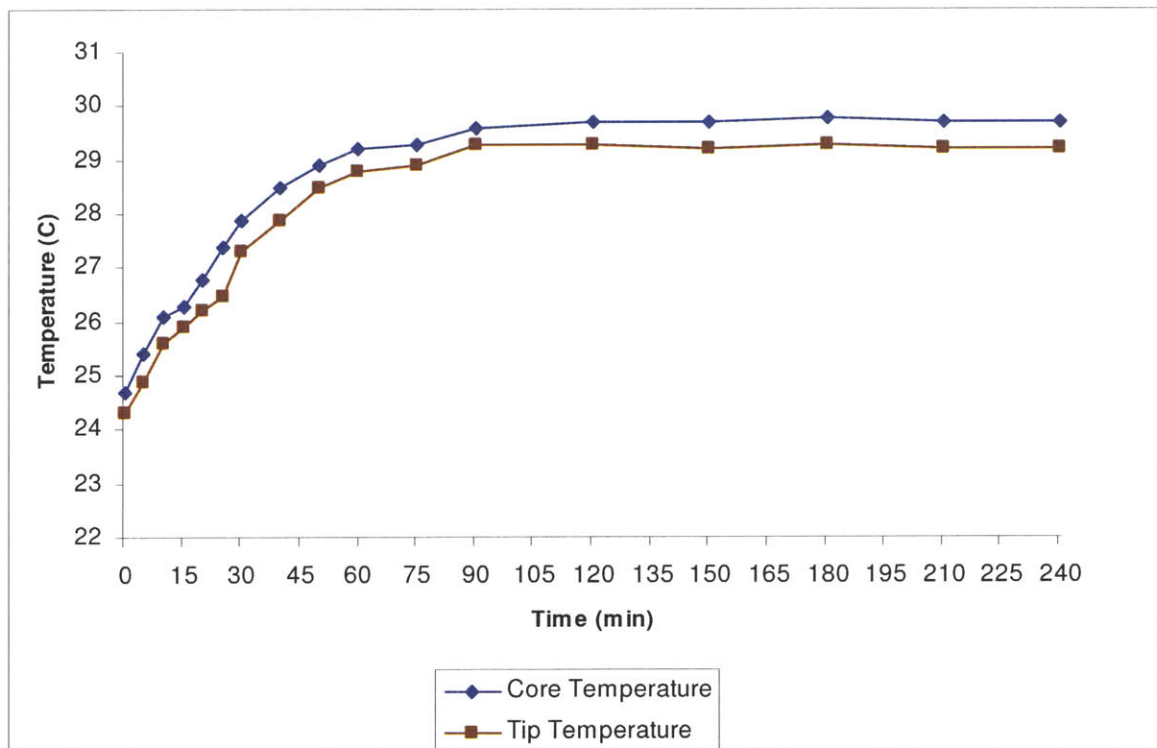
Figure 6: Temperature calibration of magnetic trap. The operating temperature for the magnetic trap's core and tip remained under 37°C.

3.3 Perfusion and Temperature Control Systems

Controlling the pH and temperature of cardiomyocytes is important since cellular dynamics are influenced by temperature and pH changes. To control the pH of the media, experiments were continuously perfused with a perfusion system. The system

was set up so that initially 75% of the volume of a 35-mm dish was filled with media. Tubes were positioned inside the dish for perfusion ensuring that the tube used for removing the media was placed much higher than the input, so that proper water level is maintained. A syringe pump (KD Scientific, MA) was used to flow media at 0.3ml/min into the dish and a peristaltic pump (Dynamax, Rainin, MA) removed it at 0.4min/ml.

A dual automatic temperature-controlled system (TC-344B, Warner Instruments) was used to maintain the temperature during the experiments close to 37°C. The operating temperature was set higher than 37°C to 39°C. Temperature measurement showed a lower temperature throughout the dish as can be seen in Figure 7. At 40°C, the average temperature around the perimeter of the dish was higher than 37°C. Thus, to avoid the possibility of cells being affected by high temperature fluctuations, 39°C was chosen as the operating temperature.

Average Temperature 37 C

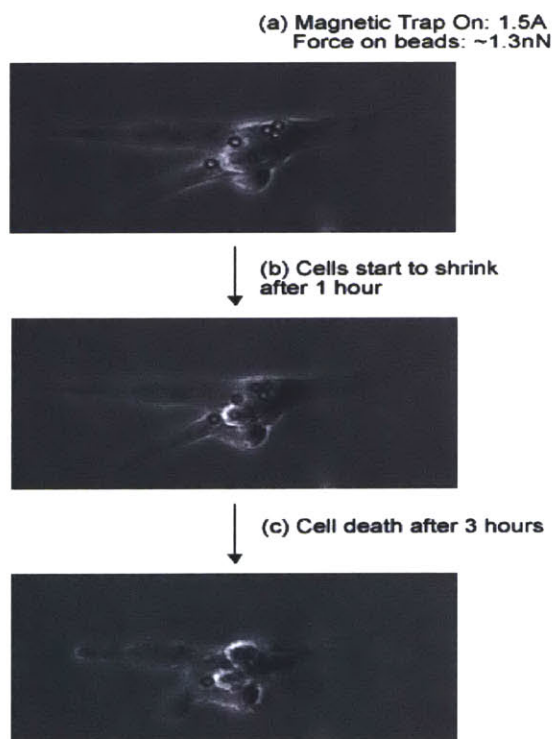**Average Temperature 39 C**
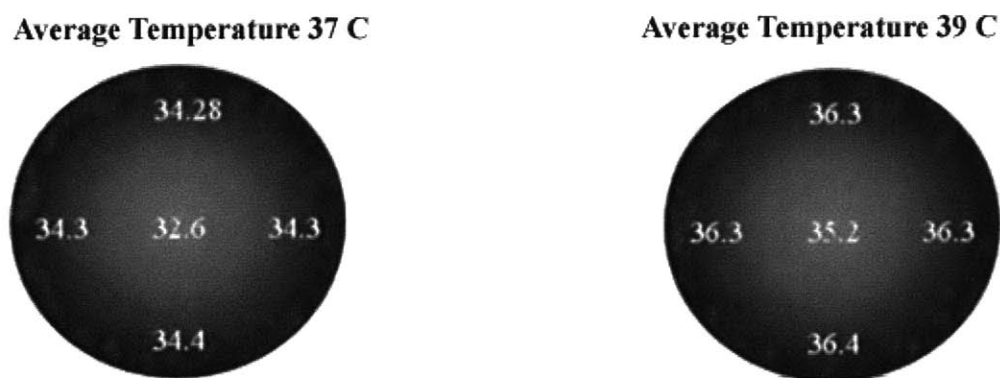
Figure 7: Temperature distribution in 35-mm dish. Operating temperature for the temperature controlled stage was set to 39°C On average the temperature was 36.3°C around the perimeter of the dish and 35.2°C at the center. Temperature measurements were averaged over 4 hours and were taken at the five locations indicated on the Figure.

Chapter 4

4.1 The Need for a Softer Substrate

Initial experiments on polystyrene plastic dishes determined that a softer substrate was needed for the system to have physiological remodeling relevance. Pulling on cells on plastic dishes resulted on cell death as shown in Figure 8. After 3 hours of pulling on beads with a force of 1.3nN in a temperature and pH controlled environment, the cells appear to have collapsed and shrunk in size. Several experiments performed on the same substrate yield the same result over 90% of the time. The substrate-cell adhesion forces were higher than expected, and the application of an external force induced a remodeling effect that ended in cellular death.

(a) Magnetic Trap On: 1.5A Force on beads: ~1.3nN

(b) Cells start to shrink after 1 hour

(c) Cell death after 3 hours

Figure 8: Magnetic trap pulling of cardiomyocytes on 35mm-polystyrene plastic dishes resulted in death. Total force exerted on cells was ~6.5nN or 1.3nN per bead.

Since the objective of the model is to study and quantify spatial and temporal remodeling effects in cardiomyocytes, a substrate that has a lower stiffness than plastic or glass is required. Several studies have suggested that polyacrylamide is an adequate substrate for mechanotransduction experiments since the stiffness of the substrate can be modified by varying the concentrations of the crosslinker, BIS, and monomer, acrylamide [66, 67]. As a result, polyacrylamide gel was selected as the substrate for the remodeling model, which yielded good experimental results, reducing interfacial stresses and allowing cells to remodel without dying.

4.2 Patterning of Polyacrylamide Gels

Patterning of polyacrylamide gels was performed as previously described by Pelham et al. and Dembo et al. [66, 67]. First, coverglasses were surface-activated for patterning polyacrylamide gels. Then, thin sheets of polyacrylamide gel were patterned on the coverglasses and a crosslinker was added to the surface of the gel for conjugation of extracellular matrix proteins.

Coverglasses (No.1, 24 x 50mm, Fisher) were sterilized with a Bunsen burner. Next, a solution of 0.1N NaOH was poured over one side of the coverglass and allowed to air dry. Afterward, 3-aminopropyltrimethoxysilane (Sigma) was poured over the treated side and incubated at room temperature for 5 minutes. The coverglasses were then thoroughly washed for 10 minutes in distilled water and incubated for 30 minutes in a 0.5% solution

of gluteraldehyde (Sigma) diluted in PBS. After incubation, the slides were washed extensively with distilled water and allowed to air dry.

10% polyacrylamide gels with 0.03% BIS were patterned on the activated glass surface. The gels were prepared by combining 3.19ml of distilled water with 1.66ml of acrylamide (30% stock solution, National Diagnostics) and 75μl of BIS (2% Stock solution, National Diagnostics). The solution was mixed and degassed for 5 minutes. Then, 25μl of a 100μg/ml ammonium persulfate solution was mixed with 2.5μl of N,N,N,N-tetramethyl ethylenediamine (TEMED, Sigma) and added to the polyacrylamide solution. A droplet of 40μl of the polyacrylamide solution was placed onto the surface of the activated coverglass and flattened with a circular cover slip (Microscope Cover Glass, 25Cir-1, Fisher). The solution polymerized within an hour; the circular coverslip was removed with a blade and a circular polyacrylamide section was patterned on the surface of the coverglass. A photoreactive crosslinker solution of Sulfo-SANPAH (1mM in 50mM HEPES, pH8.5, Pierce Chemicals) was placed on the surface of the acrylamide gel. The coverglass was placed on a UV transilluminator (FOTO/UV21, Fotodyne, WI) for 10 minutes, and the procedure was repeated. The photoreactive crosslinker reacted with proteins so that cells would pattern on the polyacrylamide surface. After photoactivation, the polyacrylamide section was washed with 50mM HEPES, pH 8.5, to remove the darkened crosslinker. The polyacrylamide sections were air-dried, sterilized with UV irradiation and stored at 4°C to be used for cell and protein patterning.

Chapter 5

5.1 Micropatterning of Cells

Controlling the number, orientation and morphology of cells is important for studies of cell biology [68-70]. When studying remodeling and conduction pathways in cardiomyocytes, it is useful to mimic the heart's architecture. The desired *in vitro* model would consist of linear arrays of myocytes spatially controlled next to one another. When seeding cardiomyocytes on a culture dish, the distribution and position of the myocytes can be influenced by the confluency of the monolayer. At low confluences, cardiomyocytes spread out and position themselves in random patterns. At high confluences, however, cardiomyocytes form dense monolayers. However, controlling the density and position of cells in these monolayers is challenging without micropatterning techniques where cell orientation and position can be dynamically controlled. For the system being developed, it is important to position cells next to each other to study the effect of gap junction coupling and how it is affected when one cell is moved with respect to another.

To overcome limitations with cell seeding techniques, several patterning techniques have been developed [70]. Photolithography has been widely used for patterning proteins on glass or silicon surfaces. However, since photolithography is expensive and is limited to planar substrates, other patterning techniques such as soft lithography have been developed [68]. Soft lithography is the use of stamps or microchannels for pattern

transfer. There are different approaches for cell and protein patterning that include microcontact printing and the use of laminar flow and microchannels for patterning [68].

In microcontact printing, a relief pattern is made on the surface of a polydimethylsiloxane (PDMS) stamp and the stamp is coated with either a solution of self-assembled monolayers (SAMs) of alkanethiols on gold or a protein solution. The "inked" stamp is then pressed onto a substrate, patterning the coated material onto selected regions of the substrate [68, 71]. Several studies have shown the efficiency of microcontact printing as specific linear pattern of cells have been produced with different cell lines including HeLa and cardiomyocytes [72].

Microfluidic channels can also be used for patterning as shown in Figure 9. By flowing fluids into a microchannel, biomolecules and cells have been selectively patterned on glass substrates and biocompatible substrates [68, 73-75]. Folch et al. used this technique to selectively patterned fibronectin and collagen proteins on surfaces, and, after removing the microchannel, seeded cells selectively attached to the patterned protein template [73]. For the purpose of our system, a similar approach will be used to take advantage of microchannels that had already been microfabricated.
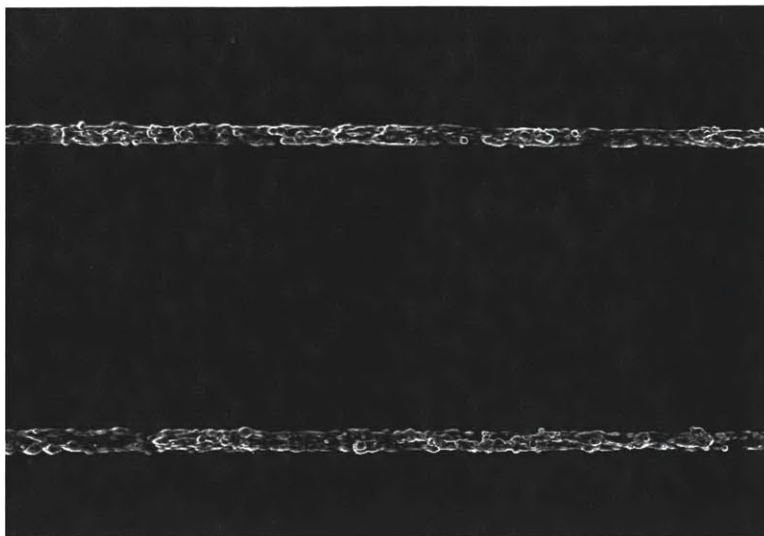
Figure 9: Cells patterned on glass substrate. Bright-field image of endothelial cells (EC) patterned on glass using microchannels of 25μm width at 4X magnification.

5.2 Fabrication of Microchannels

Microfabrication of microchannel wafers was performed at the Microsystems Technology Laboratories by Thomas Gervais (Ph.D. 2005) from Klavs Jensen's Laboratory. Silicon wafers were exposed to a photolithographic process to produce a mask to create PDMS microchannels. Master wafer contained microchannels of 2, 3 and 4mm in lengths and of 25, 50, 100μm width. These microchannels were used to determine the best dimensions for the linear strands.

A typical process to create the master silicon wafer of microchannels is as follows. First, a dark field mask is prepared with the shape and dimensions of the microchannels. A silicon wafer is dehydrated at 200°C for 1hr. SU-8 was spin coated onto the wafer, and prebaked at 105°C for 15 minutes. The mask was then used to expose an SU8 negative photoresist. Following exposure and postbake at 105°C for 15 minutes, the SU8 was

developed to remove the SU8 in the areas not exposed by the mask. The surface of the master was then cleaned, dried, and silanized for 1hr. A Polydimethylsiloxane (PDMS) mixture, consisting of a prepolymer and an initiator mixed in a 10:1 ratio, was prepared and poured over the master slide. The PDMS layer was cured at 65°C for 3hrs, and, afterwards, it was removed from the master slide. The layer was then cut along the microchannels and holes were inserted on both ends of the microchannels.

5.3 Linear Strand Patterning

To pattern the linear strands, Folch's technique was modified for patterning on poly-acrylamide gel [73]. PDMS microchannels were sterilized with 70% ethanol for 30 minutes, and heat treated for 1hr at 121.5°C in an autoclave. Although, it has become a norm to plasma sterilize the PDMS prior to patterning, this step was not performed to protect the patterned crosslinker on the polyacrylamide surface, through which the patterned extracellular matrix proteins will attach. After sterilization, the microchannels were placed on top of a dried polyacrylamide section, and were pressed down until they were firmly attached. A solution of 0.3mg/ml of fibronectin filled the microchannels. The solution was introduced by placing 40μl of the solution on one inlet of the microchannel and was introduce in the channel using a vacuum pump. The channels were then incubated for 12hr at 4°C. Any remaining solution was removed with care from the microchannel and the PDMS microchannel was pealed off from the surface of the poly-acrylamide gel. The section was then washed once with HBSS. After

thoroughly drying the section, neonatal cardiac myocytes were added. Cells selectively attach to the patterned surface and formed linear patterns as shown in Figure 10.
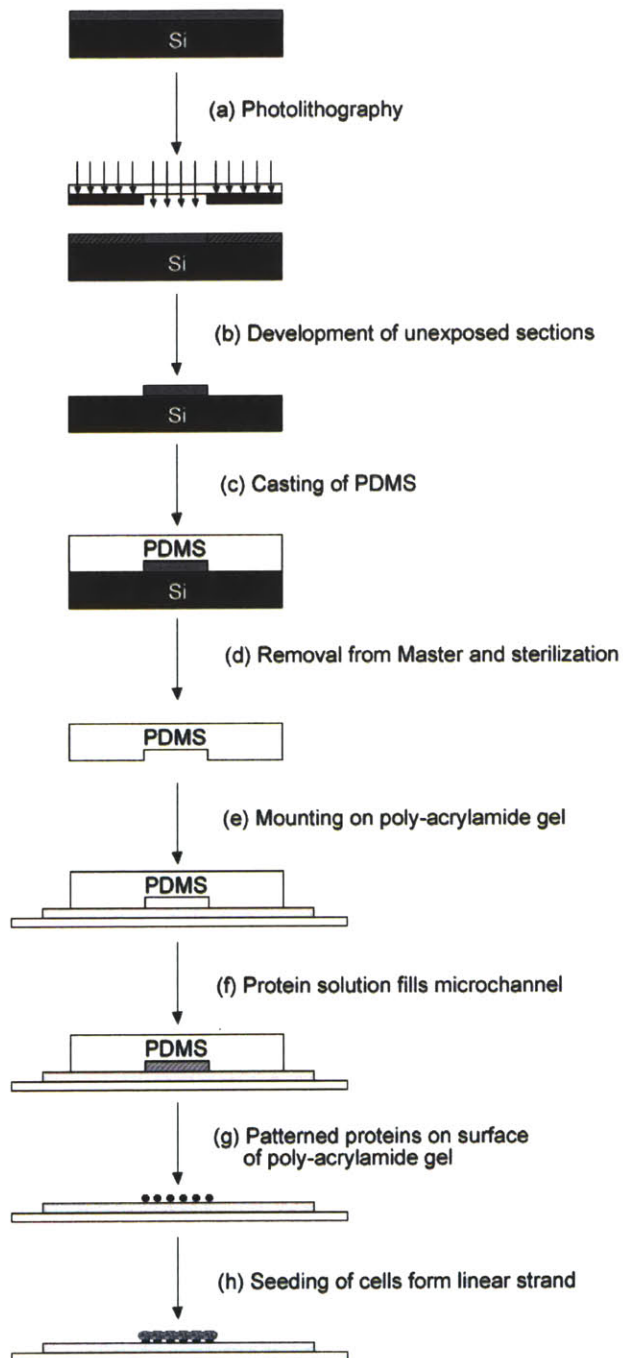
Figure 10: **Micropatterning process flow.** Steps (a) through (e) illustrate microfabrication process, while (f) through (h) illustrate patterning of extracellular proteins and cells.

5.4 Characterization of Micropatterning Process and Linear Strands

5.4.1 Micropatterning Characterization

To characterize the micropatterning process, the dimensions of the patterned linear strands were compared to the actual PDMS dimensions of the microchannel used for the patterning. Images of the linear strands and of the microchannels used for patterning were taken at 10X, 20X and 40X using an inverted light microscope (IX-70, Olympus) equipped with a digital CCD Camera (CoolSNAP, Roper Scientific). Measurements of the width of the strands, in pixels, were taken every 10μm along the length of the strand using Photoshop 7.0 (Adobe), which were then converted into microns using the parameters in table 1.

Objective	Conversion Factor (μm/pixels)
10X	0.6437
20X	0.3240
40X	0.1611

Table 1: Spatial Calibration for CoolSNAP CCD Camera

The efficiency was calculated by taking the absolute value of the ratio of the change in width size to the width of the microchannel used for patterning and subtracting it from 1 as shown by the following equation:

$$Efficiency = 1 - \left| \frac{w_{microchannel} - w_{strand}}{w_{microchannel}} \right|$$

where $w_{microchannel} - w_{strand}$ is the change in width and $w_{microchannel}$ is the width of the original microchannel on the PDMS stamp. An efficiency of 89.5% was obtained for 25μm

microchannels, whereas 50µm channels had 85.9% efficiency in patterning. Furthermore, the variance in width within the patterned strands ranged from 1µm to 8.5µm and was higher for 50µm strands. This variance can be attributed to various factors as shown in Figure 11. These factors include variation in the morphology of the PDMS microchannel, leakage of protein solution during patterning because of unevenness in polyacrylamide gel or lack of adhesion between polyacrylamide and PDMS microchannel, and diffusion of protein solution during cell seeding. Strands could also show incomplete patterning along the length of the strands.
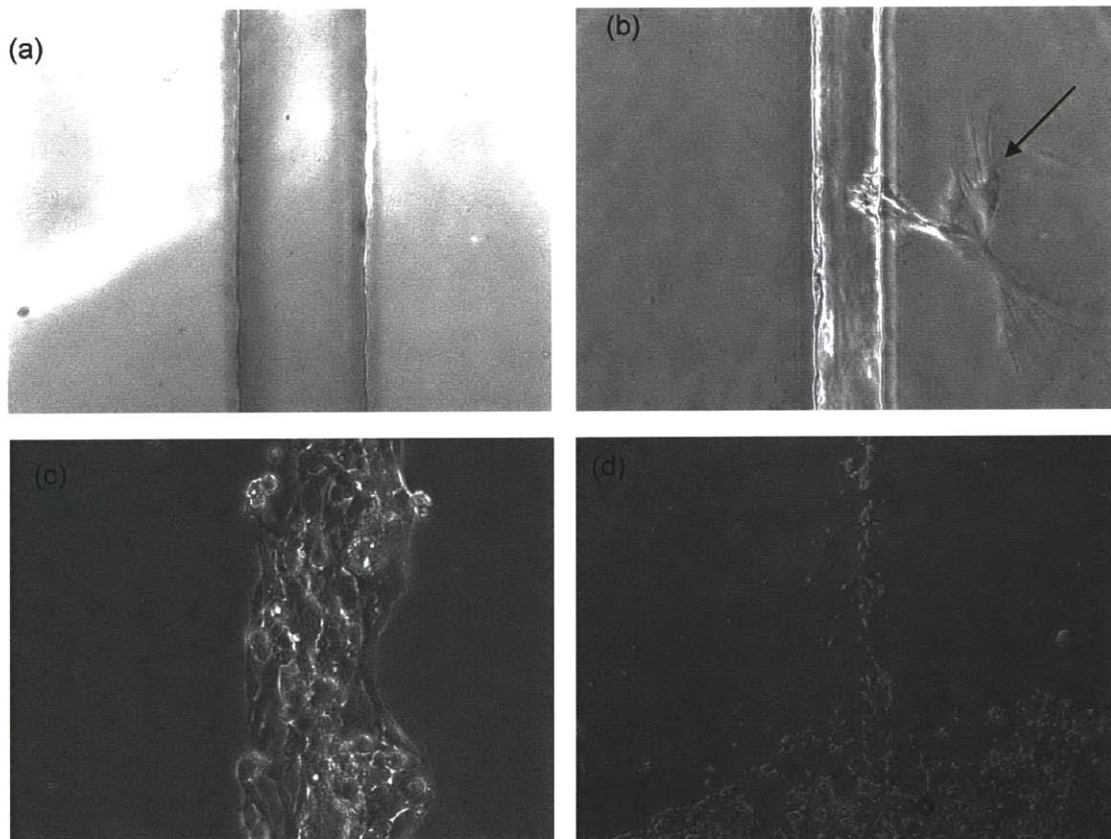
Figure 11: Factors influencing patterning of linear strand. (a) 50µm PDMS microchannel illustrates variation in morphology at 20X. (b) Dried remains of a fibronectin solution that leaked outside of 25µm microchannel at 20X. (c) Leakage almost doubles 25µm strand width at 20X. (d) Incomplete patterning of strand at 4X.

The number of cardiomyocytes along the width of the strands was as expected as Figure 12 illustrates. For a 25µm strand, 2-3 aligned along the width of the strand, since the size of cardiomyocytes is approximately 10µm. For a 50µm strand, 4-5 cells aligned along the width. Cardiomyocytes in the 25µm strand seemed to align parallel to each other along the length of the strands; whereas in a 50µm strand, cardiomyocytes aligned parallel to each other as wells as at different angles. Although the reason for this misalignment is not understood, it is expected that such an irregular alignment of cardiomyocytes can alter the anisotropic conduction within the strands, and should be avoided for impulse propagation studies. Microchannels sized greater than 50µm were not considered for the same reason.

(a)   (b)
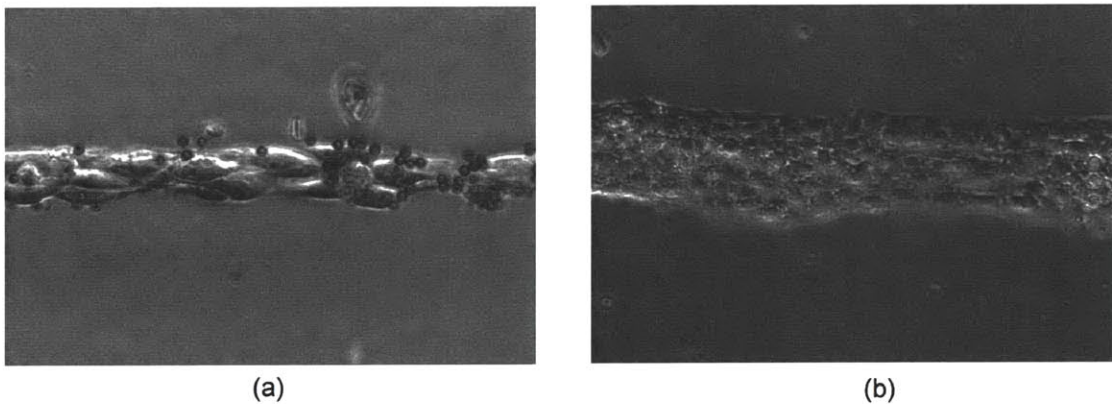
Figure 12: 25µm and 50µm linear strands. (a) Bright-field image of 25µm linear strand shown with attached Fibronectin-coated magnetic beads at 20X. (b) Bright-field image of 50µm linear strand at 20X.

Measurements in the width of the PDMS stamps after removal from the mask showed differences from the expected theoretical width. On average, 25µm microchannels had an actual width of size of 20µm ±0.5µm, and 50µm microchannels had a width size of 47µm±1.5µm. However, since the variance in width of the microchannels is small compared to the width of a cell, 10µm, there were no significant effects on the patterning.

5.4.2 Immunofluourescece Characterization of Linear Strand

Cardiomyocytes linear strands sections were fixed in 4% paraformaldehyde for 2 hours at 25°. After briefly washing in phosphate buffer saline (PBS, ph 7.4, Sigma), sections were washed in PBS-Triton-X for 1 hour. Sections were incubated in 5% goat serum blocking solution for 1 hour, and then probed with antibodies to tropomyosin (Sigma) in a 1:100 dilution for 2 hours followed by Alexa Fluor conjugated IgG1 secondary (Molecular Probes), and with connexin43 (Sigma) in a 1:100 dilution for 4 hours followed by Alexa Fluor conjugated IgM (Molecular Probes). A 1:1000 dilution of DAPI (Molecular Probes) was added last for staining of nuclei.

The strands were positive for both α-actinin and Cx43. The Cx43 distribution on the cardiomyocyte strands showed a dot-like pattern, similar to the pattern found on cells on a monolayer. Furthermore, the strands had similar characteristics to the synthetic strands of neonatal mouse myocytes described by Thomas et al. [76].
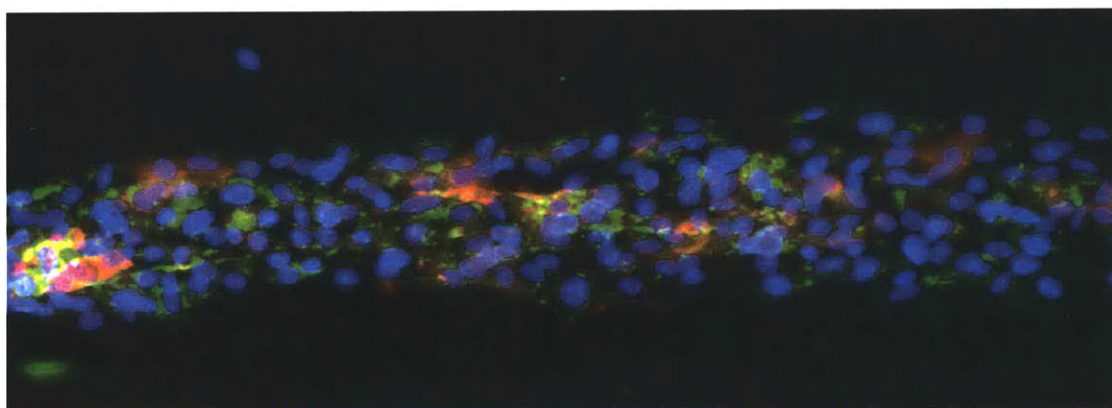
Figure 13: Neonatal cardiac linear strand stained for α-actinin and Cx43 at 20X. Cardiomyocytes are shown in red, Cx43 in green and nuclei in blue. The distribution of the gap junctions in the linear strand appears to be in a dot-like pattern around the membrane and is also seen within the cells.

Chapter 6

6.1 Experimental Setup

Chapters 3, 4, and 5 have presented the theory and characterization of each subsystem for the *in vitro* remodeling system. In this chapter, I will present the system as a whole and the methods used to study the effects of remodeling on the gap junction Cx43. In brief, to perform an experiment we isolate cardiomyocytes and pattern them into linear strands. The strands are transfected with a Cx43 fluorescent protein and after 24 hours, the strands are seeded with magnetic beads, and pulled using a magnetic trap.

6.2 Neonatal Cardiomyocytes Ventricular Isolation

Neonatal cardiomyocytes isolation was slightly modified as described in previous methods [77]. 1-2 day old Harlan Sprague-Dawley rats were used to obtained neonatal rat ventricular myocytes. The hearts were excised and washed in Hanks' balanced salt solution (HBSS, Invitrogen) and cleaned to remove the atria. They were minced and incubated in trypsin (1 mg/ml, Invitrogen) in HBSS for 3 hours at 4°C. After removing the trypsin, the resulting tissue was quickly resuspended in 1mg/ml collagenase type II (0.8 mg/ml, Worthington) in HBSS for 1 minute, followed by a second digestion of 10 minutes at 37°C. The solution was then filtered, using a 70μm cell strainer, to remove any undigested tissue, centrifuged at 800 rpm for 5 minutes to remove less dense cells such as endothelial cells and fibroblasts and then resuspended in Dulbecco's modified eagle

medium (DMEM-FBS, Invitrogen) containing L-glutamine, 7% bovine fetal calf serum (FBS, Invitrogen), 25mM Hepes Buffer, and 50 units/ml of penicillin (Invitrogen).

## 6.3 Cell Culture and Patterning of Linear Strands

Isolated cardiomyocytes were seeded on polyacrylamide gels patterned with fibronectin to form linear strands or monolayers. For a monolayer, 1 million cells were seeded on the polyacrylamide surface. For linear strands of 25μm and 50μm, sections were overseeded with 200,000 cells. The cells were cultured at 37°C and 5% CO_2, and the media was changed every 12 hours.

6.4 Purification and Transfection of Connexin43-YFP

Connexin43 yellow fluorescent fusion protein (Cx43-YFP) in the pEYFP-N1 plasmid vector (Clonetech) was obtained from D. Laird [78] and purified by my fellow student, Robin Prince. The plasmid was grown using OneShot TOP10 E.Coli chemically competent cells (Invitrogen) in 100mL of kanamycin supplemented LB medium at 37°C for 12 hours. A Maxi Prep (Maxi Kit, Qiagen) was then used to isolate and purify the grown plasmid DNA. The concentration of the purified DNA was then measured with a spectrophotometer (Smart Spec 3000, Biorad) and found to be 1.2μg/ml.

Transfection of cardiomyocytes was performed as previously described [78]. 2.2μg of plasmid DNA and 6μl of Lipofectin reagent (Invitrogen) were diluted in 100μl of Opti-

MEM1 medium (Opti, Invitrogen) and were incubated for 30 minutes at room temperature. Following incubation, both dilutions were combined and incubated for an additional 15 minutes at room temperature. Cell sections were washed with Opti-MEM1 medium prior to addition of the 200μl transfection solution. Cells were incubated for 12 hours at 37°C and 5% CO_2, after which the sections expressed Cx43-YFP as shown in Figure 14.
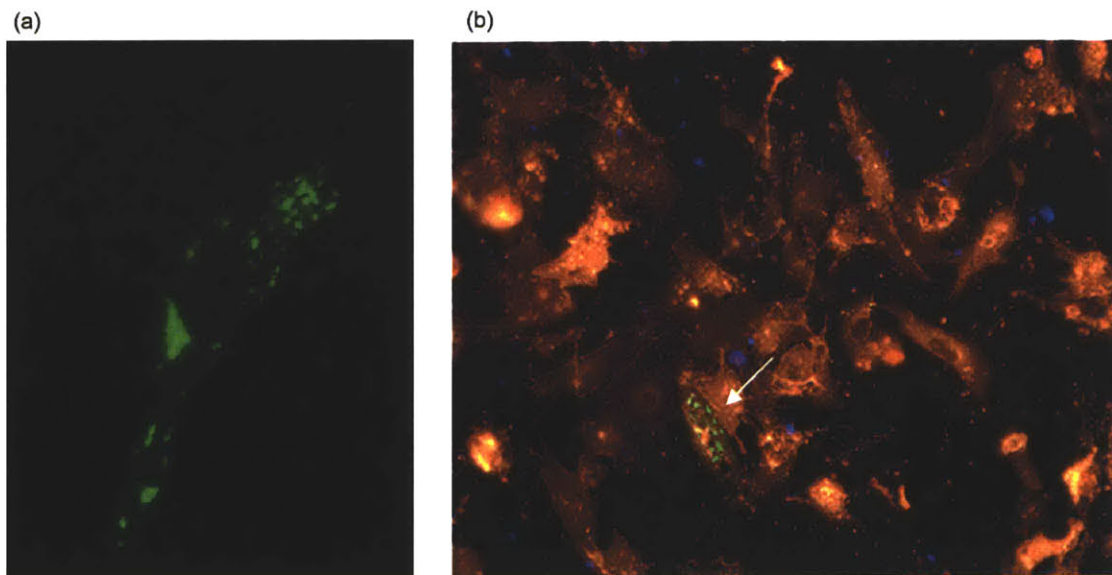
Figure 14: Cardiomyocytes transfected with Cx43-YFP. (a) Cardiomyocyte expressing Cx43-YFP 12 hours after transfection at 40X. (b) Immunofluourescece image of a transfected cell coupling with a neighboring cell at 20X. Red staining is for PKH2 red membrane cell dye (Sigma) and blue is for Hoescht (Molecular Probes).

6.5 Coating of FN-Magnetic Beads

4.5μm magnetic bead (M-450 Dynal Bead, Invitrogen) were coated with human plasma fibronectin (Invitrogen). First, 4×10^8 beads were washed in 1ml of phosphate buffered saline (PBS, Ph 7.4, Invitrogen) solution containing 0.1% bovine serum albumin (BSA).

Beads were separated from the solution with a magnet and the supernatant was discarded. The beads were then resuspended in borate buffer (pH 8.5) and 500µg of fibronectin was added. The beads were incubated for 12 hours in a rotating incubator at 37°C. The beads were washed again with PBS and stored at 4°C, until they were seeded as shown in Figure 15.
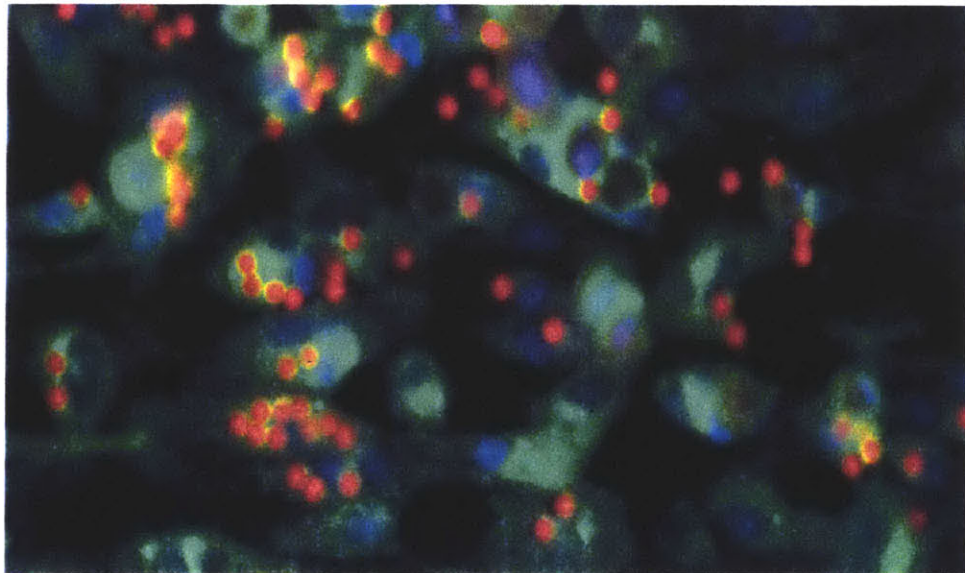
Figure 15: High-density seeding of magnetic beads on the surface of cardiomyocytes at 40X. Fibronectin-coated magnetic beads are shown in red. Cell membrane and nuclei are shown in red and blue respectively and were stained with PKH2 cell membrane linker kit and Hoescht as described in Section 6.6.1 (Sigma).

6.6 Magnetic Trap System Experimental Setup

6.6.1 Experimental Setup for Cell-to-cell Movement Experiments

Polyacrylamide sections were placed on 35-mm polystyrene dishes. A small amount of vacuum grease was applied to the bottom edges of the coverglass to avoid sliding during

imaging. Different concentrations of FN-coated magnetic beads were seeded for 30 minutes to determine the best condition for cell-to-cell movement. The concentrations were selected to reduce differences in force gradients within the imaging section, by pulling on a section with either a low or high (overseeded) density of magnetic beads. The concentrations considered were 0, 0.5×10^6, 2×10^6, and 6×10^6(overseeded). After seeding, the sections were washed with Tyrode's solution and stained for 20 minutes with PKH2 Cell Membrane Linker Kit ($4 \mu M$ PKH2 dye, $1 \mu M$ Hoescht dye, Sigma). The sections were then washed once with DMEM-FBS media to stop the labeling reaction and twice with Tyrode's solution. Afterwards, the sections were placed on a temperature-controlled stage and perfused with Tyrode's solution as described in section 6.6.2. The magnetic trap was brought to parfocal position and positioned approximately $100 \mu m$ away from the area of interest. The magnetic trap was run at 1.5A for a minimum of 2 hours. Cell-to-cell movement changes were analyzed using Photoshop 7.0 (Adobe). The reported data was collected from at least three separate experiments and reported as mean±SEM. Differences among experimental parameters were assessed using one-way ANOVA.

6.6.2 Experimental Setup for Cx43 Remodeling

Coverglasses with linear strands transfected with Cx43-YFP were mounted as described in section 6.6.1. The sections were incubated with 6×10^6 FN-coated magnetic beads for 30minutes, after which they were washed with HBSS to remove any unattached beads. Cells were overseeded with magnetic beads to induce the largest possible force, assuming

equal distribution of magnetic beads on each cell and total coverage of the cell's surface area, with 10 beads along the longitudinal axis of cell. The dishes were filled with 5ml of a 1M Tyrode's Solution (pH 7.4, Sigma), containing 20mM Hepes Buffer, and 50 units/ml of penicillin (Invitrogen), and placed on a temperature-controlled stage (TC-344B, Warner Instruments). Perfusion tubes were inserted into the dish making sure that the outflow tube was higher than the inflow, and the sections were perfused with Tyrode's solution at 0.3ml/min as described in Chapter 3. The magnetic trap was positioned approximately 100μm from the section of interest and run at 1.5A. Sections were imaged at 20X magnification with an inverted light microscope (IX-70, Olympus, Melville, NY) equipped with a motorized shutter and filter system setup for multi-filter time lapse imaging, and a high-speed piezo z-drive system for nanofocusing and scanning (P-721 PIFOC, Physik Instrumente), which was powered by an amplifier/position servo controller (E-662 LVPZT, Physik Instrumente). Image acquisition software (IPLab, Scanalytic) controlled the distance and scanning rate of the piezo objective and the exposure of the digital CCD camera (CoolSNAP, Roper Scientific MASD). The system was setup to scan 40μm z-stack, taken at 1.5μm intervals, and to acquire bright-field and FITC images at a minimum of 7 minutes per frame. Experiments lasted a minimum of 2 hours, unless interrupted by focus changes or motion artifacts. Custom MATLAB programs were written to extract images from the 40μm stack and convert them from 12-bit to 16-bit. The image that best represented the cross section of the remodeling cell was chosen for analysis.

Chapter 7

7.1 Magnetic Trap Pulling on Cells Causes Cell-to-Cell Movement

Cell-to-cell movement is believed to be an important factor leading to remodeling. In cardiac hypertrophy, enlargement of cardiomyocytes causes redistribution of gap junctions [1]. We hypothesized that local cell-to-cell movement caused by increases in stress leads to redistribution of gap junctions. For this to be examined, the magnetic trap first needed to induce cell-to-cell movement. Initial experiments on polystyrene dishes and glass slides failed to induce such motion, and lead, in general, to cell death as shown in Chapter 4.

By reducing the mechanical strains imposed on the cardiomyocytes with a polyacrylamide gel substrate, cell-to-cell motion was achieved in sections with high densities of magnetic beads. Low density seeding of magnetic beads was achieved by seeding 0.5×10^6 beads, yielding, on average, 1 bead per 11 cardiomyocytes, although the density varied. High density seeding was achieved by seeding either 2×10^6 or 6×10^6 magnetic beads, yielding on average 1 bead per 3 cardiomyocytes.

Cardiomyocytes on polyacrylamide subjected to no force displaced at a rate $0.01 \pm 0.005 \mu m/min$. Addition of magnetic beads or the presence of a magnetic field had no significant effect on the rate of displacement. Low density seeding was ineffective in producing cell-to-cell movement. The average movement of cells in a stimulated section was $0.011 \pm 0.007 \mu m/min$, which is comparable to displacement rate of non-stimulated

cells. An ANOVA analysis, with a p-value of 0.98, confirmed that the movement in low density sections was not significantly different than normal cell displacement. High density seeding, however, was more effective in producing cell-to-cell movement. In these sections, cardiomyocytes moved an average of $0.032\pm0.03\mu m/min$, faster than their normal rate. In Figure 16, for example, a cell $100\mu m$ away from the magnetic trap was pulled at 4.5nN for 2.5 hours and moved $8.9\mu m$. The result was reproducible as shown in Figure 19, where a cardiomyocyte in a linear strand was pulled $6.48\mu m$ towards the magnetic trap due to neighboring forces acting on the section. An ANOVA analysis, with a p-value of <0.0005 confirmed that the rate of displacement from high-density sections was significantly different from the rate of non-stimulated cells. Although most stimulated cardiomyocytes responded with a net motion towards the magnetic trap, some cells moved in opposite direction, presumably a result of altered overall force balance. This phenomenon was observed in cells on which a force was directly exerted upon and also on cardiomyocytes neighboring stimulated cells. .

It is important to note that due to the nature of the trap's design, there is a force gradient exerted on the strand that decreases with increasing distance. As a result, cells within the strands are pulled at different intensities, which might have effects that have not been accounted for. To eliminate this gradient, cells will need to be individually seeded, perhaps using a microinjector or some other technology that would control the position of magnetic beads on a single cardiomyocyte.
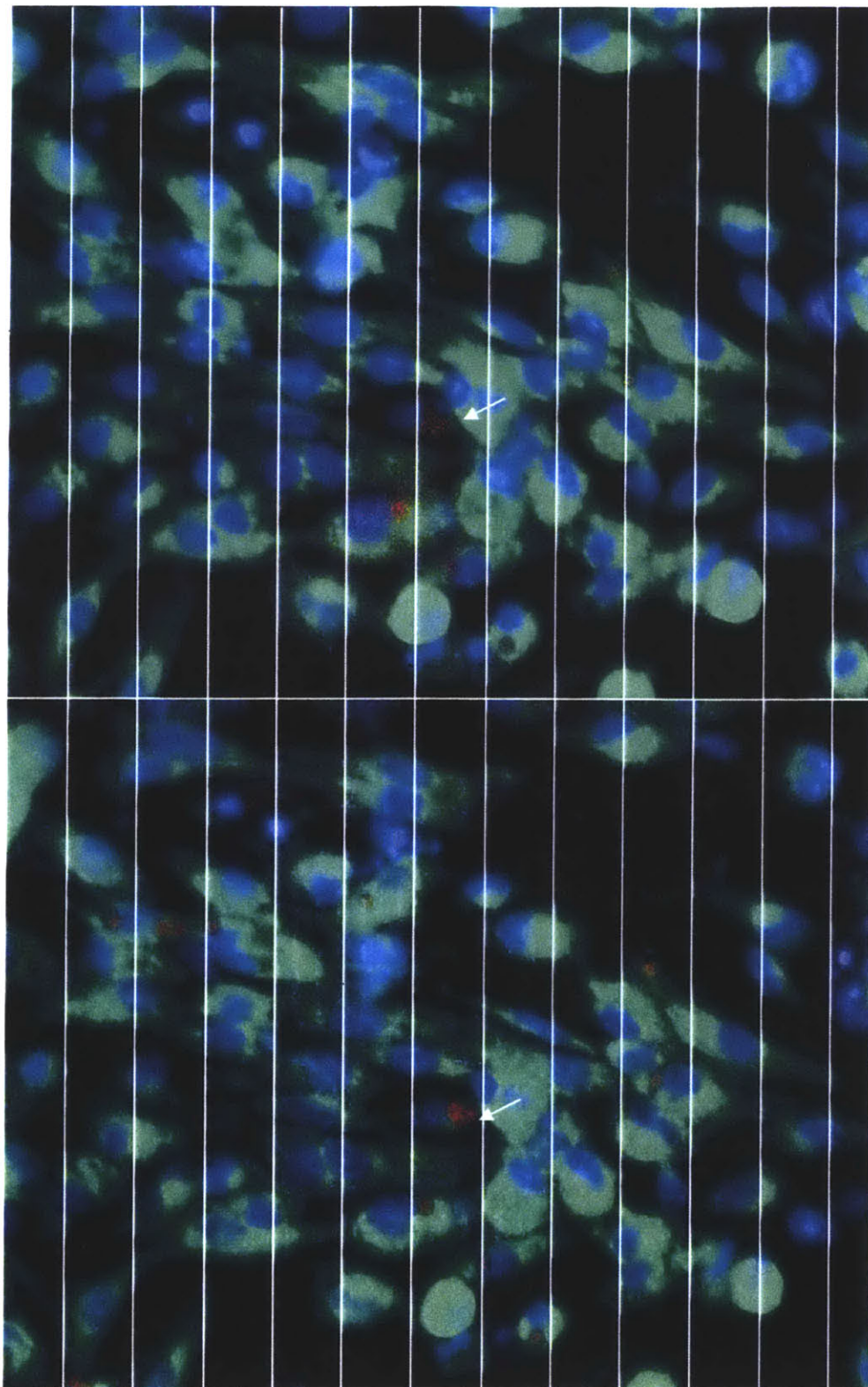
Figure 16: Cell-to-cell movement on polyacrylamide surface at 40X. Cell membrane was stained with phk4 green fluorescent membrane dye (green, Sigma) and nuclei with Hoescht dye (blue, Molecular Probes). Magnetic beads are shown in red.

7.2. Structural Remodeling of Strands Might Alter Cell-to-Cell Movement

Structural remodeling of the cells in the linear strands can influence and change the movement and displacement of cardiomyocytes subject to an external force, as well as influence gap junction remodeling. Death of cardiomyocytes within the strand might exert opposite forces on neighboring cells as they pull on the surrounding cells while they contract. Figure 17 illustrates this. Initially the top Cx43-YFP transfected cardiomyocyte is positioned at 79.4μm from the magnetic trap and is been pulled at 2.01nN. Although the cell exhibits a brief initial net motion towards the magnetic trap, remodeling of the strands left of the transfected cell causes the cell to be displaced in opposite direction, moving away from the magnetic trap. We would have expected the cell to move approximately 4.5μm after 2.5 hours; however, the cell moved 5.2μm from its original position away from the magnetic trap, despite the magnetic trap exerting an average force of 1.9nN.

Apoptosis of a cell can also occur even without an applied force. Cell death can naturally occur and might depend on the lifespan of the cells (isolated neonatal cardiomyocytes typically last up to 5 days or more), the viability of the cell isolation, media conditions, temperature changes, confluency of cells in the strand or monolayer and metallic ions that might leak from the magnetic trap's iron core or metallic coatings due to magnetic bead collisions at the tip. Cells might also respond to the exerted force by moving in opposite direction to counter the external force, although this was rarely seen in sections patterned on polyacrylamide gel.
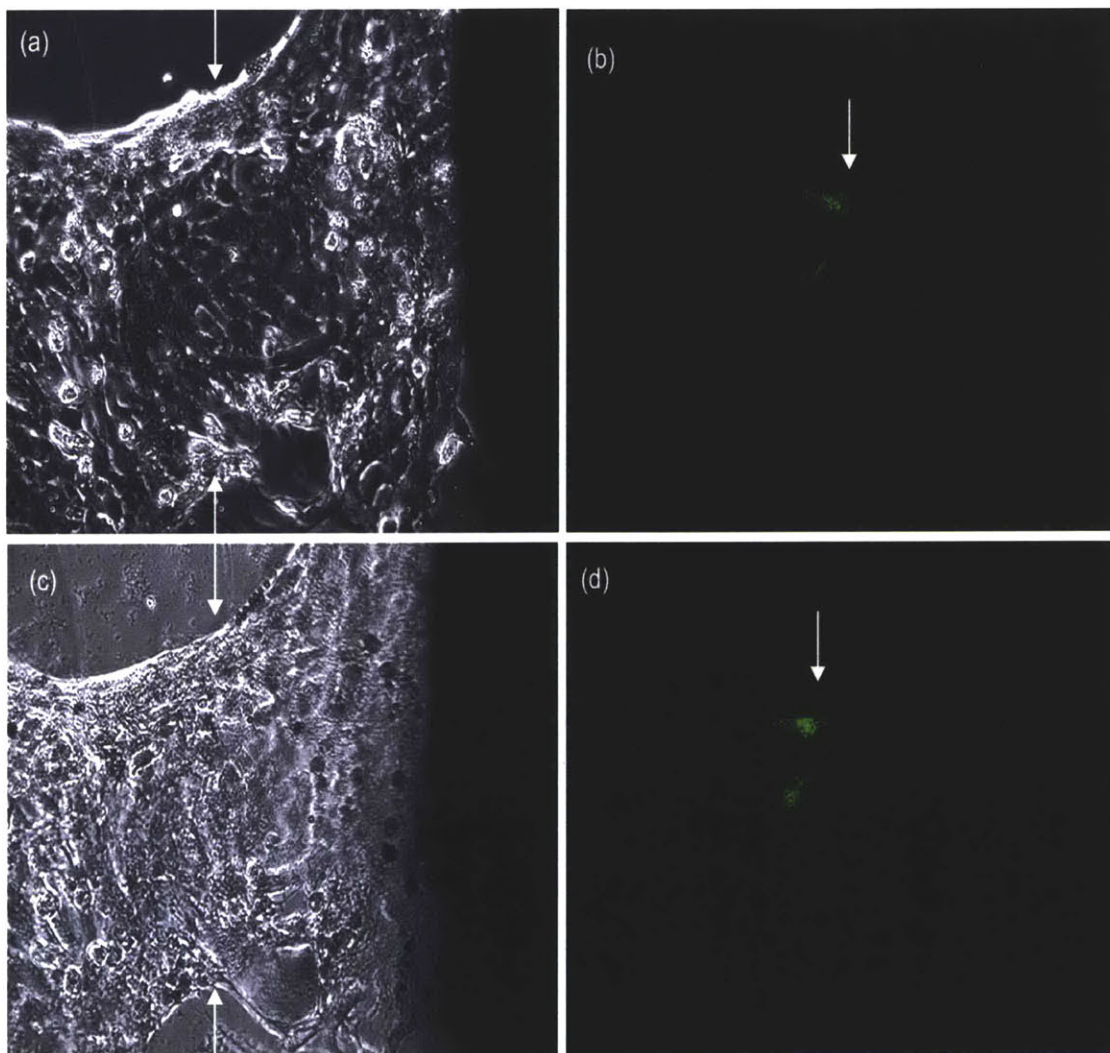
Figure 17: Structural remodeling of a linear strand causes cardiomyocytes to move in opposite direction. (a) Initial bright-field image of transfected section at 20X. (b) Initial fluorescent image of Cx43-YFP transfected cells at 20X. (c) After 2.5 hours, cells within the strand die, rearranging the structure of the strand. The width of the strand changes by 20µm, indicating that at least two or more cardiomyocytes have collapsed, shrunk, and most likely die. (d) Remodeling of the linear strand causes cells to move away from the magnetic trap.

7.3 Localized Applied Forces Cause Remodeling of Connexin43 in Cardiomyocytes

Once cell-to-cell movement of the cardiomyocytes was achieved, the next step was to study remodeling of cardiomyocytes. The hypothesis proposed was that when cardiomyocytes move, the gap junctions undergo remodeling. Initial experiments with the magnetic trap system repeatedly produced remodeling of the Cx43-YFP by exerting local and controllable mechanical forces on cardiomyocytes. For instance, in Figure 17, the Cx43 distribution within the transfected cardiomyocyte changes. Cx43 initial expression is widely distributed throughout the entire cell surface. After 2.5 hours of stimulation, the Cx43 expression shifted towards the right edge of the cell, where it locally increased its expression. Although, in this experiment the movement and displacement of the cells were influenced by structural remodeling of the strand, the changes in Cx43 seemed to indicate that in response to local stresses, the system could induce remodeling of the gap junctions. Subsequent experiments further demonstrated that the applied local forces can induce a remodeling effect on Cx43.

A change in Cx43 expression was observed in an overseeded monolayer of cardiomyocytes, with approximately 3 magnetic beads per cell. A local applied force caused a cell to bulge and push against a transfected cell. This increase in local stress deformed the cell membrane of the transfected cell and produced a local transient upregulation of Cx43 expression at that cell border as shown in Figure 18. The upregulation was relatively short, lasting less than 12 minutes, and quickly downregulated after the bulge disappeared. This intriguing result suggested that local applied forces can, in addition to remodeling the gap junctions, regulate the expression

levels of connexins. This fact is further supported by Zhuang et al. who showed that a pulsatile stretch upregulated Cx43 expression [32].
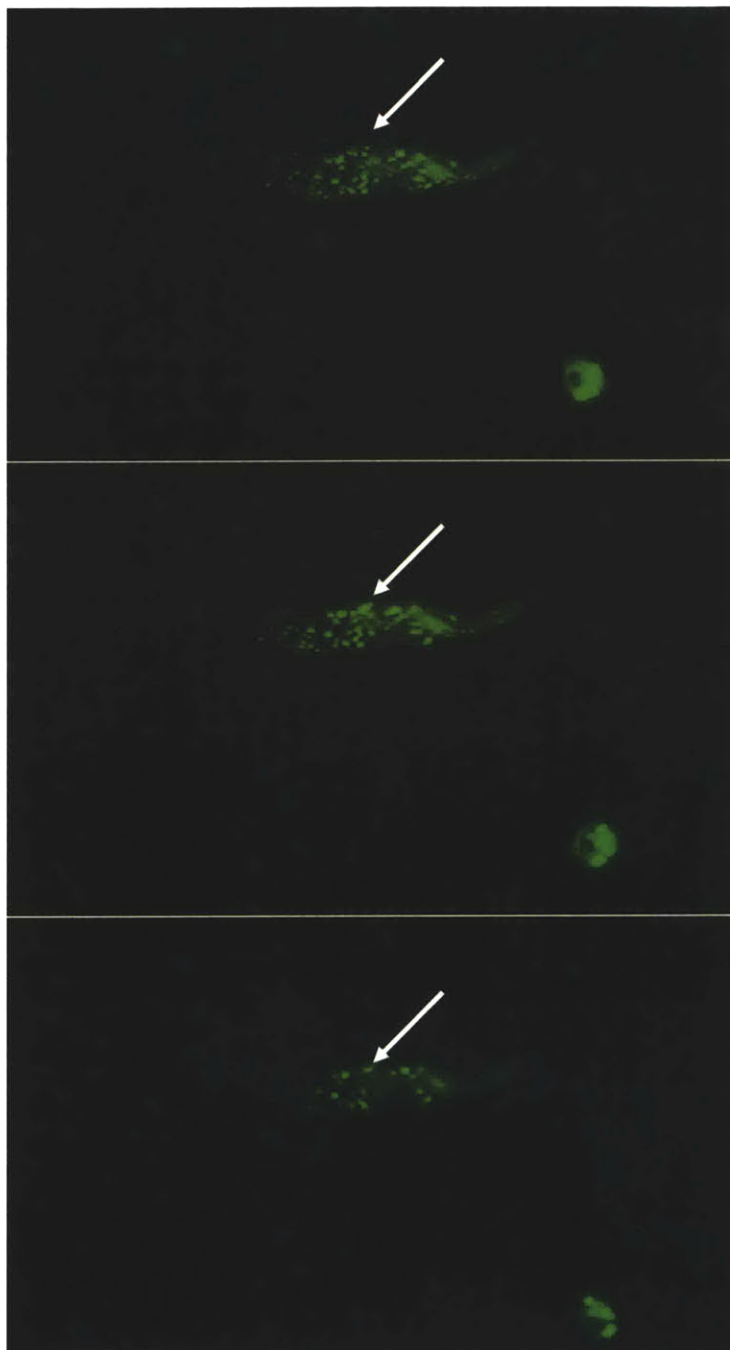
Figure 18: Transient upregulation of Cx43 at 40X. After 1 hour of stimulation, a cell to the top left of the transfected cardiomyocyte bulges and produces a transient upregulation of Cx43 that lasted 24 minutes.

To determine whether applied forces could lead to temporal upregulation and/or downregulation of Cx43, linear strands were overseeded with magnetic beads. As cardiomyocytes were pulled towards the magnetic trap, cell-to-cell movement caused Cx43 remodeling. It was clear that local remodeling of the gap junctions occurred over time as Cx43 expression changed locations within the cell. It could not be established, however, if after 2 hours the total protein expression of Cx43 was upregulated or downregulated. For instance, in Figure 19, a transfected cardiomyocyte displaced 6.5μm shows signs of both upregulation and downregulation as the cell displaces and moves against other cardiomyocytes within the strand. Initially, connexin expression is mostly located on the right area of the cell. After 30 minutes, connexins remodel and redistribute evenly around the perimeter of the cell. Further stimulation leads to more dynamic changes in the distribution of the connexins, until they reposition parallel to the top cell membrane, and their expression is increased. This dynamic spatial and temporal remodeling of the gap junctions shows that cell-to-cell movement is possible with this system and that it leads to changes in gap junctional distribution and remodeling of cardiomyocytes. We cannot conclude, however, if local applied forces lead to the upregulation or downregulation of total cell Cx43 expression. To precisely quantify the levels and changes of connexin expression, photobleaching effects need to be evaluated. We believe that photobleaching does not play a significant role in the results we have presented since changes in Cx43 distribution have been detected throughout time; however we need to determine to what extent photobleaching affects the intensity in the connexin expression. Furthermore, since connexin expression also depends on spatial distribution, three-dimensional protein distribution needs to be quantified to assess if

connexin expression increased, decreased or remained constant throughout the cell or if the changes are at a specific areas within the cell. These and other considerations will be further recommended as future work.
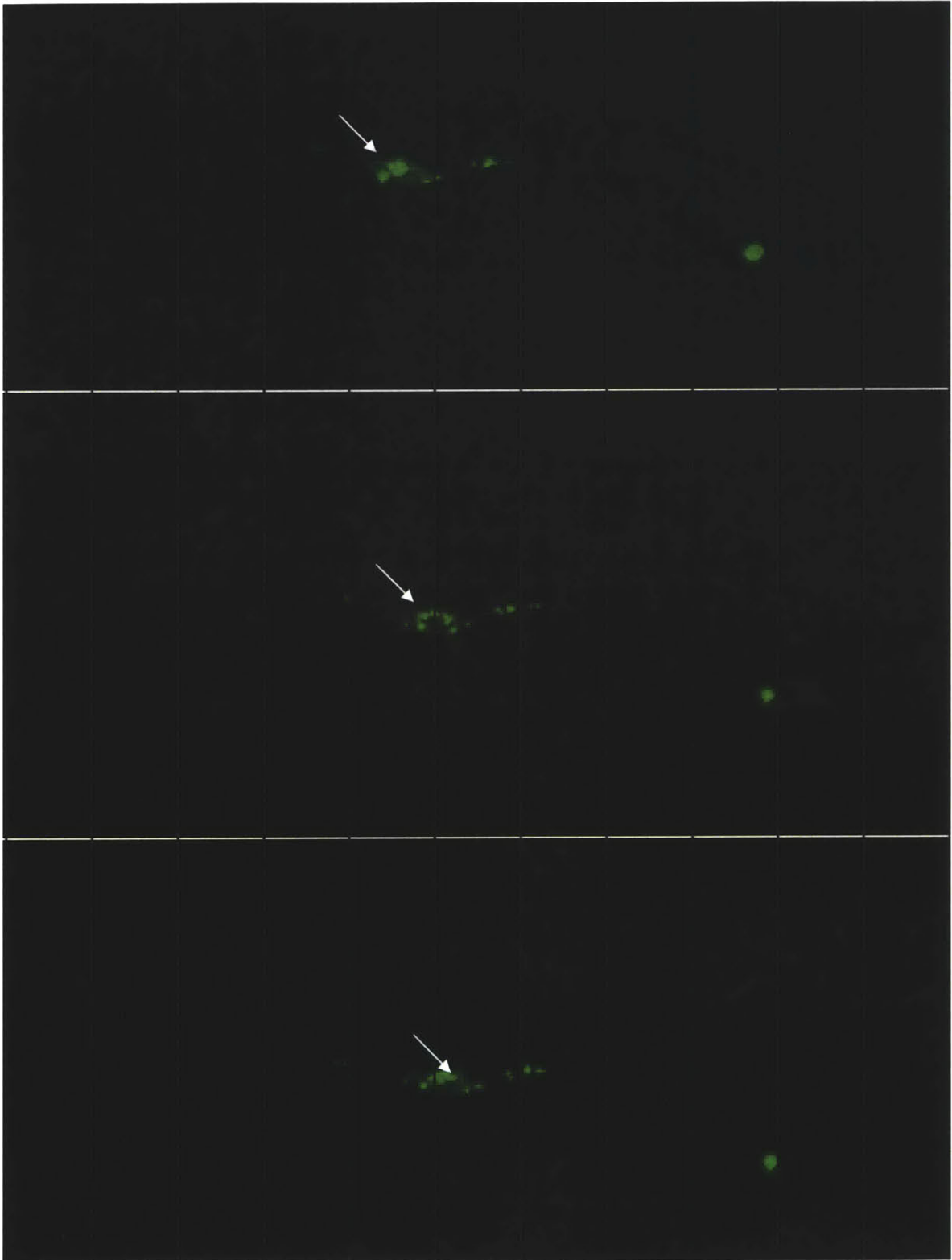
Figure 19: Redistribution of Cx43 as gap junctions remodel as cell displaces at 20X. Initially, Cx43 is located on the left area of the cell; then, shifts and redistributes along the perimeter of the cell, and finally localize parallel to the membrane.

Chapter 8

The development of a force micromanipulation remodeling system is a powerful tool for cardiovascular research. Research with this technology would lead to further understanding of gap junction remodeling, and provide insights into cardiac remodeling, reentry circuits and anisotropic conduction changes in the presence of increase local stresses.

8.1 Future Studies on Connexin43 Remodeling and Impulse Propagation

Since the long term objective is to be able to quantify how a single local force on a transfected cardiomyocyte disturbs connexin expression, force gradients need to be minimized. Control of the spatial distribution of the force will require improvements on the bead seeding technique. One possibility includes the use of a microinjector system to position and control the distribution of the beads on a cell.

Subsequent studies will be directed to quantify how variations in force intensity lead to changes in Cx43 expression and three-dimensionally remodeling of the gap junctions. It would also be physiologically relevant to determine if changes in the angle of the applied force have a significant effect on connexin remodeling, since alterations to the longitudinal and transverse location of the connexins will affect the anisotropy of the strand. This could be assess by quantifying Cx43 remodeling when a cell is pulled in the longitudinal direction along the long axis, or transversally. This model could also be applied to study effects of local forces on anisotropic conduction and impulse propagation.

References

1. Kostin, S., Dammer, S., Hein, S., Klovekorn, W.P., Bauer, E.P., Schaper, J., *Connexin 43 expression and distribution in compensated and decompensated hypertrophy in patients with aortic stenosis.* Cardiovascular Research, 2004. **62**(2): p. 426-36.

2. Jongsma, H.J., Wilders, R., *Gap Junctions in Cardiovascular Disease.* Circulation Research, 2000. **86**: p. 1193-1197.

3. Dhein, S., Jongsma, H.J., *Forming the Network-gap junctions in the cardiovascular system* Cardiovascular Research, 2004. **62**: p. 225-227.

4. Roberts, R., *Principles of Molecular Cardiology.* Hurt's The Heart, ed. V. Fuster, Alexander, R.W., O'Rourke, R.A. 2001, New York: Mc-Graw Hill. 95-113.

5. Sohl, G., Willecke, K., *Gap Junctions and the connexin protein family.* Cardiovascular Research, 2004. **62**: p. 228-232.

6. Polontchouk L., H.J.A., Ebelt B., Schaefer T., Sthulmann D., Mehlhorn U, et al. , *Effects of chronic atrial fibrillation on gap junction distribution in human and rat atrial.* Journal of the American College of Cardiology, 2001. **38**: p. 883-91.

7. Van der Velden H.M., J.H.J., *Cardiac gap junction and connexins: their role in atrial fibrillation and potential therapeutic targets.* Cardiovascular Research, 2002. **54**(270-279).

8. Stains J.P., C., R., *Gap Junctions in skeletal development and function.* Biochimica et Biophysica Acta, 2005. **1719**: p. 69-81.

9. Berg, J.M., Tymoczko, J.L., Stryer, L., *Gap junctions allow ions and small molecules to flow between communicating cells.* Fifth ed. Biochemistry. 2002, New York: W.H. Freeman and Company. 364-365.

10. Moreno, A., *Biophysical properties of homomeric and heteromultimeric channels formed by cardiac connexins.* Cardiovascular Research, 2004. **62**: p. 276-286.

11. Berthoud, V.M., Minogue, P.J., Laing, J.G., Beyer, E.C., *Pathways for degradation of connexins and gap junctions.* Cardiovascular Research, 2004. **62**: p. 256-267.

12. Vaidya, D., Tamaddon, H.S., Lo, C.W., et al. , *Null mutation of connexin43 causes slow propagation of ventricular activation in the late stages of mouse embryonic development.* Circulation Research, 2001. **88**: p. 1196-1202.

13. Gustein, D.E., Morley, G.E., Tamaddon, H. et al. , *Conducion slowing and sudden arrhythmic death in mice with cardiac-restricetd innactivation of connexin 43* Circulation Research, 2001. **88**: p. 333-339.

14. Schulz, R., Heusch, G., *Connexin43 and ischemic preconditioning.* Cardiovascular Research, 2004. **62**: p. 335-344.

15. Rohr, S., *Role of gap junctions in the propagation of the cardiac action potential.* Cardiovascular Research, 2004. **62**: p. 309-322.

16. Van Veen, T.A.B., Van Rijen, H.V.M., Opthof, T., *Cardiac gap junction channels: modulation of expression and channel properties.* Cardiovascular Research, 2001. **51**: p. 217-229.

17.   Spach, M.S., Heidlage, J.F., Dolber, P.C., Barr, R.C., *Electrophysiological effects of remodling cardiac gap junctions and cell size: Experimental and model studies of normal cardiac growth.* Circulation Research, 2000(86): p. 302-311.

18.   Reed K.B., W., E.M., Larson, D.M., et al., *Molecular cloning and functional expression of human connexin37, an endothelial cell gap junction protein.* Journal of Clinical Investigation, 1993. **91**: p. 997-1004.

19.   Delorme, B., Dahl, B., Jarrry-Guichard, T., et al. , *Developmental regulation of Connexin40 gene expression in mouse heart correlates with the differentiation of the conduction system.* Developmental Dynamics, 1995. **204**: p. 358-371.

20.   Coppen, S.R., Dupont, E., Rothery, S., Severs, N.J., *Connexin45 expression is preferentially associated with the ventricular conduction system in mouse and rat heart.* Circulation Research, 1998. **82**: p. 232-243.

21.   Lerner, D.L., Yamada, K.A., Schuessler, R.B., Saffitz, J.E., *Accelerated onset and increased incidence of ventricular arrhythmias induced by ischemia in Cx43-deficient mice.* Circulation, 2000. **101**: p. 547-552.

22.   Nikolski, V.P., Jones, S.A., Lancaser, M., *Cx43 and Dual-Pathway Electrophysiology of the Atrioventricular Node and Atrioventricular Nodal Reentry.* Integrative Physiology, 2003. **92**: p. 469.

23.   Kwak, B.R., van Kempen, M.J.A., Thevenia-Ruissy, M., Gros, D.B., Jongsma, H.J. , *Connexin expression in cultured neonatal rat cardiomyocytes reflect the pattern of the intact ventricle.* Cardiovascular Research, 1999. **44**: p. 370-380.

24.   Peters, N.S., *New insights into myocardial arrhythmogenesis: Distribution of gap-junctional coupling in normal, ischaemic and hypertrophied human hearts.* Clinical Sciences (Colch), 1996. **90**: p. 447-452.

25.   Kleber, A., *Intercellular Communication and Impulse Propagation.* Cardiac Electrophysiology: From Cell to Bedside, 2004. **Chapter 24**: p. 213-231.

26.   Rudy, Y., *Ionic Mechanisms of Cardiac Electrical Activity: A Theoretical Approach.* Fourth ed. Cardiac Electrophysiology: From Cell to Bedside, ed. D. Zipes, Jalife, J. 2004, Philadelphia: Saunders. 255-266.

27.   Shaw, R.M., Rudy, Y., *Ionic mechanisms of propagation in cardiac tissue: Roles of the sodium and L-type calcium currents during reduced excitability and decreased gap junctional coupling.* Circulation Research, 1997. **81**: p. 727-741.

28.   Wang, Y., Rudy, Y. , *Action potential propagation in inhomogeneous cardiac tissue: Safety for considerations and ionic mechanism.* American Journal of Physiology: Heart and Circulatory Physiology, 2000. **278**: p. H1019-H1029.

29.   Fast, V.G., Kleber, A.G., *Microscopic conduction in cultured strands of neonatal rat heart cells measured with voltage-sensitive dyes.* Circulation Research, 1993. **73**: p. 914-925.

30.   Spach, M.S., Heidlage, J.F., *The stochastic nature of cardiac propagation at a microscopic level-electrical description of myocardiacl architecture and its application to conduction.* Circulation Research, 1995. **76**: p. 366-380.

31.   Kleber, A.G., Jansen, M.J., Fast, V.G., *Normal and abnormal conduction in the heart.* In page E, Fozzard, H.A., Solaro, R.J ed. The Handbook of Physiology, ed. . 2002, New York: Oxford University Press.

32.   Zhuang, J., Yamada, K.A., Saffitz, J.E., Kleber, A.G., *Pulsatile stretch remodels cell-to-cell communication in cultured myocytes.* Circulation Research, 2000. **87**: p. 316-322.

33.   Poelzing, S., Akar, F.G., Baron, E., Rosenbaum, D.S., *Heterogeneous connexin43 expression produces electrophysiological heterogeneities across ventricular wall.* American Journal of Physiology: Heart and Circulatory Physiology, 2004. **286**: p. H2001-H2009.

34.   Eloff, B.C., Lerner, D.L., Yamada, K.A., Schuessler, R.B., Saffitz, J.E., Rosenbaum, D.S., *High resolution optical mapping reveals conduction slowing in connexin43 deficient mice.* Cardiovascular Research, 2001. **4**: p. 681-690.

35.   Kanno, S., Saffitz, J.E., *The role of myocardial gap junctions in electrical conduction and arrythmogenesis.* Cardiovascular Research, 2001. **10**: p. 169-177.

36.   Lerner, D.L., Beardslee, M.A., Saffitz, J.E., *The role of altered intercellular coupling in arrhythmias induced by acute myocardial ischemia.* Cardiovascular Research, 2001. **50**(2): p. 263-269.

37.   Bastide, B., Neyses, L., Ganten, D. et al. , *Gap junction protein connexin40 is preferentially expressed in vascular endothelium and conductive bundles of rat myocardium and is increased under hypertensive conditions.* Circulation Research, 1993. **73**: p. 1138-1149.

38.   Peters, N.S., Green, C.R., Poole-Wilson, P.A., Severs, N.J., *Reduced contenct of connexin43 gap junctions in ventricular myocardium from hypertrophied and ischemic human hearts.* Circulation, 1993. **88**: p. 864-875.

39.   Wang, X., Gerdes, A.M., *Chronic pressure overload cardiac hypertrohpy and failure in guinea pigs.* Journal of Molecular Cell Cardiology, 1999. **31**: p. 333-343.

40.   Severs, N.J., *The cardiac muscle cell.* Bioessays, 2000(22): p. 188-199.

41.   Uzzaman, M., Honjo, H., Takagishi, Y., et al., *Remodeling of gap junctional coupling in hypertrophied right ventricles of rats with monocrotaline-induced pulmonary hypertension.* Circulation Research, 2000. **86**: p. 871-878.

42.   Sepp, R., Severs, N.J., Gourdie, R.G., *Altered patterns of intercellular junction distribution in human patients with hypertrophic cardiomyopathy.* Heart, 1996. **93**: p. 10933-10938.

43.   Smith, J.H., Green, C.R., Peters, N.S., Rothery, S., Severs, N.J., *Altered patterns of gap junction distribution in ischemic heart disease.* American Journal of Pathology, 1991. **139**: p. 801-821.

44.   Kaprielian, R.R., Gunning, M., Dupont, E., et al, *Downregulation of immunodetectable connexin43 and decreased gap junction size in the pathogenesis of chornic hibernation in the human left ventricle.* Circulation, 1998. **97**: p. 651-660.

45.   Smith, J.H., Green, C.R., Peters, N.S., Rothery, S., Severs, N.J., *Disturbed connexin43 gap junction distribution correlates with the location of reentrant circuits in the epicardial border zone of healing canine infarcts that cause ventricular tachycardia.* Circulation, 1997. **95**: p. 988-996.

46.   Beardslee, M.A., Lerner, D.L., Tadros, P.N. et al., *Dephosphorylation and Intracellular Redistribution of Ventricular Connexin43 During Electrical Uncoupling Induced by Ischemia.* Circulation Research, 2000. **79**: p. 115-127.

47. Toyofuku, T., Yabuki, M., Otsu, K., et al, *Functional role of c-Src in gap junctions of the cardiomyopathic heart.* Circulation Research, 1999. **85**: p. 672-681.

48. Matsushita, T., Oyamada, M., et al., *Remodeling of cell-cell and cell-extracellular matrix interactions at the border zone of rat myocardial infarcts.* Circulation Research, 1999. **85**: p. 1046-1055.

49. Sadoshima, J., Izumo, S., *The cellular and molecular response of cardiac myocytes to mechanical stress.* Annual Review of Physiology, 1997. **59**: p. 551-571.

50. Walsh, R.A., *Molecular and cellular biology of the normal hypertrophied and failing heart.* Hurst's The Heart, ed. V. Fuster, Alexander, R.W., O'Rourke, R.A. 2001, New York: McGraw-Hill.

51. Marian, A.J., *Pathogenesis of diverse clinical and pathological phenotypes in hypertrophic cardiomyopathy.* Lancet, 2000. **355**(9197): p. 58-60.

52. Zuppinger, C., Schaub, M.C., Eppenberger, H.M., *Dynamics of early contact formation in cultured adut rat cardiomyocytes studied by N-cadhering fused to green fluorescent protein.* Journal of Molecular Cell Cardiology, 2000. **32**: p. 539-555.

53. Polontchouk L., E., B., Jackels, M., Dhein, S., *Chronic effects of endothelin-1 and angiotensin II on gap junctions and intercellular communication in cardiac cells.* The FASEB Journal, 2001. **16**(1): p. 87-89.

54. Dodge, S.M., Beardslee, M.A., Darrow, B.J., Green, K.G., Beyer, E.C., Saffitz, J.E., *Effects of angiotensin II on expression of the gap junction channel protein connexin43 in neonatal rat ventricular myocytes.* Journal of American College of Cardiology, 1998. **32**: p. 800-807.

55. Pimentel, R.C., Yamada, K.A., Kleber, A.G., Saffitz, J.E., *Autocrine regulation of myocytes Cx43 expression by VEGF.* Circulation Research, 2002. **90**: p. 671-677.

56. Saffitz, J.E., Kleber, A.G., *Effects of mechanical forces and mediators of hypertrophy on remodeling of gap junctions in the heart.* Circulation Research, 2004. **94**: p. 585-591.

57. Hill, J., *Electrical Remodeling in Cardiac Hypertrophy.* Trends in Cardiovascular Medicine, 2003. **13**: p. 316-322.

58. Armoundas, A.A., Wu, R., Juang, G. et al., *Electrical and Structural remodeling of the failing ventricle.* Pharmacological Therapy, 2001. **92**: p. 213-230.

59. Wasson, S., Reddy, H.K., Dohrmann, M.L., *Current perspectives of electrical remodeling and its therapeutic implications.* Journal of Cardiovascular Pharmacology and Therapeutics, 2004. **9**(2): p. 129-144.

60. Mow, V.C.G.F., Tran-Son-Tay, Hochmuth, R.M., *Cell Mechanics and Cellular Engineering.* 1994, New York: Springer Verlag

61. Bausch, A.R., Moller, W., Sackmann, E., *Measurement of local viscoelasticity and forces in living cells by magnetic tweezers.* Biophys. J., 1999. **67**: p. 818-827.

62. Brown, T.D., M. Bottlang, D.R., Pedersen, A.J. Banes, *Loading paradigms-intentional and unintentional- for cell culture mechanostimulus.* The american journal of the medical sciences, 1998. **316**(3): p. 162-168.

63. Huang, H., Dong, C.Y., Kwon. H., Sutin, J.D., Kamm, R.D., So. P.T.C., *Three-Dimensional Celllar Deformation Analysis with a Two-Photon Magnetic Manipulator Workstation.* Biophysical Journal, 2002. **82**: p. 2211-2223.

64. Lammerding, J., Kazarov, A.R., Huang, H., Lee, R.T., Hemler, M.E., *Tetraspanin CD151 regulates alpha-6-beta-1 integrin adhesion strengthening.* PNAS, 2003. **100**(13): p. 7616-7621.

65. Halliday, D., Resnick, R., Krane, K.S., *Ampere's Law.* Fourth ed. Physics. Vol. 2. 1992, New York: John Wiley & Sons, Inc.

66. Dembo, M., Wang, Y., *Stresses at the cell-to-substrate interface during locomotion of fibroblasts.* Biophysical Journal, 1999. **76**: p. 2307-2316.

67. Pelham, R.J., Wang, Y., *Cell locomotion and focal adhesions are regulated by substrate flexibility.* PNAS, 1997. **94**: p. 13661-13665.

68. Kane, R.S., Takayama, S., Ostuni, E., Ingber, D.E., Whitesides, G.M., *Patterning proteins and cells using soft lithography.* Biomaterials, 1999. **20**: p. 2363-2376.

69. Sighvi, R., Kumar, A., Lopez, G.P., Stephanopoulos, G.N., Wang, D.I., Whitesides, G.M., Ingber, D.E., *Engineering cell shape and function.* Science, 1994. **264**(5159): p. 696-698.

70. Nishizawa, M., Takoh, K., Matsue, T., *Micropatterning of HeLa Cells on Glass Substrates and Evaluation of Respiratory Activity Using Microelectrodes.* Langmuir, 2002. **18**: p. 3645-3649.

71. Kam, L., Shain, W., Turner, J.N., Bizios, R., *Axonal outgrowth of hippocampal neurons on micro-scale networks of polylysine-conjugated laminin.* Biomaterials, 2000. **22**: p. 1049-1054.

72. Kaji, H., Takii, Y., Nishizawa, M. , Matsue, T., *Pharmacological characterization of micropatterned cardiac myocytes.* Biomaterials, 2003. **24**: p. 4239-4244.

73. Folch, A., Toner, M., *Cellular micropatterns on biocompatible materials.* Biotechnology Progress, 1998. **14**: p. 388-392.

74. Delamarche, E., Bernard, A., Schmid, H., Michel, B., Biebuyck, H., *Microfluidic networks for chemical patterning of substrates: designand application to bioassays.* Journal of American Chemistry Society, 1998(120): p. 500-508.

75. Delamarche, E., Bernard, A., Schmid, H., Michel, B., Biebuyck, H., *Patterned delivery of immunoglobulins to surfaces using microfluidic networks.* Science, 1997. **276**: p. 779-781.

76. Thomas, S.P., Biercher-Lehmann, L., Thomas, S.A., Zhuang, J., Saffitz, J.E., Kleber, A.G., *Synthetic Strands of Neonatal Mouse Cardiac Myocytes.* Circulation Research, 2000. **87**: p. 467-473.

77. Yamamoto, K., Dang, Q.N., Kennedy, S.P. Osathanondh, R., Kelly, R.A., Lee, R.T., *Induction of Tenascin-C in Cardiac Myocytes by Mechanical Deformation: Role of Reactive Oxygen Species.* Journal of Biological Chemistry, 1999. **247**(31): p. 21840-21846.

78. Jordan, K., Solan, J.L., Dominguez, M., Sia, M., Hand, A., Lampe, P.D., Laird, D.W., *Trafficking, Assembly, and Function of a Connexin43-Green Fluorescent Protein Chimera in Live Mammalian Cells.* Molecular Biology of the Cell, 1999. **10**(6): p. 2033-2050.

Appendix

A.1 MATLAB Programs

A. 12-BIT to 16-BIT Stack Converter

MATLAB code to convert 3D image stack taken with IP Lab into single .tif image files.

```
% stack_converter
% Use for extracting data from IP Lab zstack
% Extracts .tiff files from a .tiff stack
% Converts each file to 16bit
% Frames saved in same directory

clear
[filename, pathname]=uigetfile('*.*','Select Image Stack');
if filename
    cd(pathname);
    file=fullfile(pathname,filename);
    [path,name,ext]=fileparts(filename);
    info=imfinfo(file);
    stacksize=length(info)
    for i=1:stacksize
        image_12bit=imread(file,i);
        image_16bit=bitshift(image_12bit,4);
        imwrite(image_16bit, [name '_' num2str(i), '.tif'], 'tif');
    end
end
```

B. Average Intensity of an Area over Time

MATLAB code to calculate the average intensity of an area over time.

```
%Program for obtaining the average intensity over time of a selected area
%in a sequence of frames.

function [low_intensity, max_intensity, number_frames, out]=area_intensity(directory)

%getting into directory
cd(directory);
dr=dir('*.tif');
dr={dr.name};
n=size(dr,2);
```

```matlab
number_frames=n;

%get single file and parameters
pic=imread(dr{1});
[X Y image Rect]=imcrop(pic);
image_width=X(1,2);
image_lenght=Y(1,2);
x_position=Rect(1,1);
y_position=Rect(1,2);
area_width=Rect(1,3);
area_lenght=Rect(1,4);
figure, imshow(image);
rect=Rect;
x_position
y_position

for i=1:n
    file=imread(dr{i});
    [x y intensities square]=imcrop(file,rect);
    mean_per_column=mean(intensities);
    average_mean=mean(mean_per_column);
    average_data(:,i)=average_mean;
end

low_intensity=min(min(average_data))
max_intensity=max(max(average_data))
out=average_data

frames=[1:n];
time=frames/13;
data_points=average_data(1,:)
subplot(2,1,1), plot(average_data);
xlabel('frames');
ylabel('pixel_intensities');
subplot(2,1,2), plot(time,data_points);
xlabel('time(sec)');
ylabel('pixel_intensities');
axis([0 5 (low_intensity-5) (max_intensity+5)]);
```